Betti Carolina (Orcid ID: 0000-0001-7384-6494)
Quiroga Mónica (Orcid ID: 0000-0001-8056-5383)
Lederhos Cecilia (Orcid ID: 0000-0002-4537-4810)

Role of the Support and Chloride During the Purification of 1-Pentene in Alkyne/Alkene Streams over Pd Catalysts

*Misael Cordoba[1,4], Carolina Betti[1], Luciana Martínez Bovier[1], Lina García[1,3], Fernando Coloma-Pascual[2], Alfonso Ramírez[4], Mónica E. Quiroga[1,5], Cecilia R. Lederhos[1,]**

[1] *Instituto de Investigaciones en Catálisis y Petroquímica, INCAPE (FIQ-UNL, CONICET), Colectora Ruta Nac. N° 168 Km 0, Pje El Pozo, 3000 Santa Fe, Argentina.*

[2]*Servicios Técnicos de Investigación, Facultad de Ciencias, Universidad de Alicante, Apartado 99, E-03080 Alicante, Spain.*

[3]*Grupo de Investigación Ciencia e Ingeniería en Sistemas Ambientales (GCISA), Facultad de Ingeniería Civil, Departamento de Ing. Ambiental, Universidad del Cauca, calle 5 Nº 4-70, 1900 Popayán, Colombia.*

[4]*Grupo de Investigación en Catálisis. Universidad del Cauca, Calle 5 Nº 4-70, 1900 Popayán, Colombia.*

[5]*Facultad de Ingeniería Química, Universidad Nacional del Litoral, Santiago del Estero 2829, 3000 Santa Fe, Argentina.*

** Tel.:+54 (342) 451-1370/1546 Int. 6109. E-mail: clederhos@fiq.unl.edu.ar*

Abstract

BACKGROUND: Pd nanoparticles over different supports were evaluated during the alkyne selective hydrogenation of medium chain (C_7 and C_5) and the 1-pentene purification at mild operational conditions (150 kPa and 303 K). The role of support and chloride was investigated; γ-Al_2O_3, γ-Al_2O_3 modified with Mg, $CaCO_3$ and activated carbon were used as supports and $PdCl_2$ as precursor salt. The classical Lindlar catalyst was used as reference.

RESULTS: The surface acidity offered by supports: weak, intermediate and strong acid sites (electronic effects), dispersion (geometric effects), surface species: MgO, $Pd_xCl_yO_z$ and/or functional groups (electronic effects); they can favor or disfavor the desorption of 1-alkene during

This article has been accepted for publication and undergone full peer review but has not been through the copyediting, typesetting, pagination and proofreading process which may lead to differences between this version and the Version of Record. Please cite this article as doi: 10.1002/jctb.6755

the purification of 1-pentene stream and the alkyne selective hydrogenation. Smallest particle sizes (3.8- 10.0 nm) favor the dissociative adsorption of hydrogen over Pd° active sites promoting good catalytic behavior. The best synthesized catalysts are Pd/Al–Mg and Pd/Ca, their high selectivity (≥ 90 %) is favored by the presence of superficial acidic Lewis sites. On the contrary, lower selectivity (74-80%) is assessed on catalysts with Brönsted acidic sites (Pd/Al and Pd/RX3), that favored the undesired overhydrogenation or isomerization reactions.

CONCLUSION: The role of the support, the geometric and electronic properties during the hydrogenation reactions have the major influence on the selectivity and the catalytic performance. Low loaded Pd catalysts supported on Al_2O_3-Mg and $CaCO_3$ (Pd/Al-Mg, Pd/Ca) can be used for the purification of medium or large terminal alkenes at mild reaction conditions as an alternative to the toxic Lindlar commercial catalyst.

Keywords: Selective Hydrogenation, Alkyne, Palladium Nanoparticles, Support, Alkene Purification.

INTRODUCTION

The selective catalytic hydrogenation of alkynes has as its main product alkenes, due to the wide variety and versatility of alkenes application. Alkenes are very important products of the Fine Chemistry, Petrochemistry and Polymer Industry, etc[1, 2]. They are produced by non-selective thermal processes (steam cracking) or catalytic cracking of naphtha fractions, and are separated into cuts containing predominantly molecules of a specified number of carbon atoms. However, each cut contains the multiply unsaturated impurities (alkynes and dienes), so the problem is to purify the alkene stream using solvents (not environmentally friendly) or by selective hydrogenation reaction using a catalyst (green-chemistry process). This hydrogenation reaction is a key process for the elimination of impurities due to obtaining products with high added value. Selective hydrogenation reactions of short-chain alkynes (acetylene, propyne, butyne) have been studied extensively[3, 4], due

to several applications of the obtained products. The understanding about the hydrogenation of medium or long chain compounds is of great importance[5-7], however the behavior of these systems is still under study. In this context, several authors have studied reactions of selective hydrogenation of medium/high molecular weight alkynes (C_5 – C_7)[6,8-10], 3-methyl-1-pentyn-3-ol[11], 2-methyl-3-butyn-2-ol[12], phenylacetylene[13] and others[14].

Additionally, several authors have studied the alkenes production from petrochemical streams containing alkyne and alkadiene impurities[15-18], these compounds need to be removed before the alkene is used in polymerization processes[16, 19, 20]. The presence of alkynes between 10 – 0.01 vol % in olefin streams are undesirable because they diminish the quality of polymer, and also, alkyne poisons the used catalysts in polymerization processes[21]. For example, a high purity alkene stream (polymer grade) for Ziegler-Natta catalyzed polyalkene formation must be essentially free from alkynes; usually, for a 1-butene stream; maximum desirable concentration of methylacetylene (plus other acetylenes) is 10 ppm in volume[16].

In the last decades, reports were focused in terms of controlling the selectivity during the hydrogenation of alkynes to obtain either pure alkenes or enriched alkenes streams. Selective processes in catalytic hydrogenation using heterogeneous catalysts can be affected by one or more factors that determine what type of catalyst should be used. In this sense, adjusting these parameters in the best way can generate the best synergism between catalytic activity and selectivity. Generally, the parameters that are directly related to improve the selectivity in the catalysts can be divided into structural properties and/or electronic properties. These parameters could be related to the following factors: the active phase, particle size, pore volume, structure and surface composition, surface acidity.

Palladium catalysts are very used in hydrogenation reactions due to its high hydrogenating capacity, being an active and selective phase at low temperature and pressure[6, 22, 23]. However, the overhydrogenation should be avoided. The classical Lindlar catalyst, consisting of $Pd_{(5\%)}/CaCO_3$ poisoned with lead (which greatly increases its selectivity), has been used since 1954[24, 25]. This

catalyst presents some disadvantages such as: i) its high cost due to the high metallic loading, ii) impossibility to pelletize preventing its removal and reuse, and iii) restricted use, especially for the manufacture of food, cosmetic and medicine, since the leaching of extremely toxic lead compound occurs. So, there is a challenge of synthesizing new low cost catalysts improving the performance of Lindlar catalyst with comparable or higher selectivity to the desired product during hydrogenation processes of medium/large molecular weight alkynes. Several Pd catalysts have been prepared and evaluated for the selective hydrogenation of olefins, e.g. $Pd_{(1\%)}$/Hydrotalcite[26], Pd_4S/carbon nanofiber[18] and different bimetallic catalysts, $Pd_{(0.4\%)}$-$Ni_{(0.5\text{-}1\%)}$[22], $Pd_{(0.5\%)}$ - $In_{(0.4\%)}$[27], $Pd_{(1\text{-}5\%)}$ - Bi[28].

Kiwi-Minsker et al.[29] discussed the role of support in the selective hydrogenation of alkynes. Although the immediate role of the support is to dilute the active phase and facilitate the handling of the catalyst, the good choice of the suitable support also represents a powerful tool that will influence the properties of the catalyst[30]. In fact, the support provides some control of the particle size, the distribution of the metal and the stability of the active phase. Furthermore, the chemical and electronic properties generated due to metallic sites and support interactions, improves the catalyst performance[31]. While its structural properties affect the diffusion and adsorption of reagents and desorption of generated products[32]. Different supports, like metal oxides (TiO_2, Al_2O_3, Fe_3O_4, MgO, $CaCO_3$ and MnO_2), or metal-organic frameworks (MOF), or activated carbon (C) are widely used synthesizing catalysts for the selective hydrogenation of alkynes[6, 33-35]. To optimize the performance of catalysts, it is essential to understand the effect of the support on the catalytic activity during the selective hydrogenation reaction. On the other hand, to study the effect of the residual chloride species of the chlorinated precursors is of great importance in the purification processes. These species can intervene in the catalytic activity and in the sulfurresistance processes by the presence of these compounds in these streams. In previous work during the selective hydrogenation of styrene with different catalysts, it was found that chloride complex species ($Pd_x^{\delta+}O_yCl_z$) present in the surface electronic and steric effects that improved the activity or the

sulfur resistance[36-38]. However, the effect of the acidity, residual chloride species and surface properties of the support on the catalytic performance has not been investigated in detail for selective hydrogenation of medium/long chain alkynes neither for the purification of alkene/alkyne mixtures. In a previous work, low loaded Pd catalysts were prepared using chloride of tetraamminepalladium(II) $[Pd(NH_3)_4]Cl_2$ as a precursor solution. Highly dispersed Pd nanoparticles were obtained with an average particle size between 3−4.5 nm. The results of purification of 1-pentene and hydrogenation of 1-heptyne or 1-pentyne showed high activity and selectivity for the prepared catalysts. Selectivity values were indeed higher than those of the Lindlar commercial catalyst[15].

Based on the above considerations, the objectives of this work are: i) Synthesize and characterize Pd catalysts using different supports γ-Al_2O_3, γ-Al_2O_3 modified with Mg, $CaCO_3$ and a activated carbon obtained by incipient wetness impregnation of $PdCl_2$. ii) Evaluate the supported Pd catalysts during the purification of 1-pentene in an alkyne/alkene (1-pentyne/1-pentene) stream and the selective hydrogenation of medium chain terminal alkynes (C_7 and C_5) reaction at mild operational conditions. iii) Study the effects of the acid strength of the catalysts, the type of active sites, particle sizes and the residual chloride, over the activity and selectivity. iv) Compare the activity and selectivity of the synthesized catalysts in contrast to those obtained with the classic Lindlar catalyst at identical operational conditions.

EXPERIMENTAL

Catalyst Preparation

Four materials were used as support in this study: $CaCO_3$ (Anhedra, purity 98.6%), activated carbon NORIT- RX3 EXTRA (acid-washed, steam-activated carbon powdered) and γ-Al_2O_3 (CK-300, Ketjen powdered, mesh 35-80, previously calcined 3 h at 823 K). RX3 and $CaCO_3$ were used without previous treatment. A fraction of alumina was treated with an aqueous solution of

$MgSO_4.7H_2O$ (Anhedra, purity 99.8 %) in order to obtain ca. 5 wt % of Mg, dried 24 h at 373 K and calcined for 3 h at 823 K. Solids were called Al_2O_3 and Al_2O_3-Mg, respectively.

Pd/Al, Pd/Al-Mg, Pd/Ca and Pd/RX3 catalysts were obtained by incipient wetness technique. The impregnation was performed using a solution of $PdCl_2$ (Aldrich, purity 99.0 %) at pH= 1 for alumina or carbonaceous supports, while pH=5 was used for $CaCO_3$ support. The solutions were stirred and sonicated during 20 min at 42 kHz and 100W (using a Branson Ultrasonics 2510 equipment). The final charge on the catalysts was ca. 1 wt % of Pd. Then, the synthetized monometallic catalysts were dried at 393 K during 24 h. Samples on Al_2O_3 and Al_2O_3-Mg were calcined in air at 873 K for 3 h; while the samples on $CaCO_3$ and RX3 were pretreated with a N_2 flow during 3 h at 873 K in order to stabilize palladium nanoparticles, and avoid the support decomposition in an inert atmosphere. Finally, all the catalysts were reduced 1 h at 573 K in a H_2 stream at 50 mL min^{-1} in a tubular continuous flow quartz reactor.

Catalysts Characterization

A Micromeritics ASAP 2020 instrument was used to obtain the nitrogen adsorption-desorption isotherms between 0.02 and 0.98 relative pressures (P/P_o) and the Brunauer–Emmett–Teller (BET) model was used to calculate the specific surface area (S_{BET}) of the supports. Samples were outgassed 2 h at 523 K under vacuum, and then N_2 adsorption isotherms at 77 K were obtained.

The mass content of Pd in the catalysts was determined by Atomic Emission Spectroscopy with Inductive Plasma (ICP-OES) using a Perkin Elmer OPTIMA 2120 equipment, after digestion of the samples in diluted sulfuric acid solution at 363 K.

The acidic strength and also amounts of acid sites on the surface of the alumina and carbonate based supports and catalysts, were measured by Temperature Program Desorption using pyridine as a probe molecule (TPD-Py). Measurements were made in a tubular reactor coupled to a Shimadzu GC-8A gas chromatograph with FID detector. Before the analysis 200 mg of the samples were *ex situ* reduced at 573 K for 30 min. The solids were then put into a fixed bed reactor treated with

constant 40 mL min^{-1} of N_2 flow at 723 K to desorb physisorbed compounds. The samples were cooled up to room temperature, and were treated during 30 min with a flow of nitrogen saturated with pyridine (Merck, Purity 99.5 wt %). After that, the weakly physisorbed pyridine was removed at 418 K for 1 h, at 40 mL min^{-1} constant N_2 flow. Then, the temperature was increased from 418 up to 1000 K at a heating rate of 10 K min^{-1}. The gases issued by the reactor were directly sent to the methanator and analyzed with a flame ionization detector (FID). The signal of the detector was recorded continuously versus the temperature of the sample.

The acidic properties (Brönsted and Lewis acid sites ratio) of the supports and catalysts were evaluated by *in- situ* means of Diffuse Reflectance Infrared Fourier Transform Spectroscopy of pyridine (DRIFT-Py) in a Shimadzu FTIR, Affinity-1S. 25 mg of each sample was heated *in situ* in the cell for 30 min under vacuum at 673 K. The cell was cooled up to 423 K and the background spectrum was recorded. Nitrogen saturated with Pyridine at atmospheric pressure was then introduced into the cell at 423 K for 30 min. All measurements were performed at this temperature to prevent physisorption of pyridine. The sample was then heated for 30 min at 473 K, cooled down up to 423 K and the spectrum was recorded by averaging 64 scans with a resolution of 4 cm^{-1}.

Surface chemistry of the activated carbon support was quantified in DTA/TGA-TA Instruments SDT Q600 coupled to a Hiden Mass Spectrometer 0-200 amu, 10 mg of the sample was heated from 278 to 1273 K and a ramp of 20 K min^{-1} in He atmosphere at a flow of 100 mL min^{-1}. The area under the peaks of CO, CO_2 and O_2 desorptions were determined by the deconvolution using the Fityk programme. The reductive character of surface species was evaluated by Temperature Programmed Reduction analysis (TPR-H_2). The measurements were made in Micromeritics Auto Chem II equipment equipped with a thermal conductivity detector. Before the analysis the samples were subjected to a pretreatment in Ar at 673 K for 30 min, and then cooled up to room temperature. The reduction procedure was carried out using a mixture of 5 % H_2/Ar at a flow rate of 30 mL min^{-1} with a heating ramp of 10 K min^{-1} up to 1273 K. The metal particle diameter and their distributions were obtained by TEM using a JEOL 100 CX II electron microscope with an

acceleration voltage of 100 kV and 270000x. The samples were prepared by grinding the pellets, suspending the particles in ethanol and then sonicating them during 15 min. A drop of this suspension was placed on a 200 mesh copper grid with a Formvar film and observed in the equipment. A set of digital images were taken in order to make the phases identification and measure the particle diameters. Digital Micrograph software was used to obtain the particle size distributions. The electronic state of surface species and their superficial atomic relationships were obtained by X-Ray Photoelectron Spectroscopy (XPS), following the Pd $3d_{5/2}$, Ca $2p_{3/2}$, and 2p peak position of Mg, Cl and Al. The measurements were made using a VG-Microtech Multilab instrument equipped MgK_{α} ($h\upsilon$: 1253.6 eV) and an energy flow of 50 eV. The analysis pressure during data acquisition was maintained at 5.10^{-7} Pa. The samples were *ex situ* previously reduced 1 h at 573 K in H_2 flow, following the same pretreatment conditions. The areas of the peaks were estimated by calculating the integral of each peak after subtracting a Shirley background and fitting the experimental peak to a combination of Lorentzian/Gaussian lines of 30–70% proportions. The binding energy used as reference were the Al 2p at 74.7 eV, Ca $2p_{3/2}$ at 346.6 eV and C 2p at 284.6 eV, respectively for the Al_2O_3, $CaCO_3$ and C supports[39]. The crystalline structure of the catalysts was defined in an X-ray Diffraction (XRD) Shimadzu XD-D1 equipment, with a CuK_{α} (λ = 1.5405 Å) in the range $10 < 2\theta < 85^{\circ}$, at 1° min^{-1} scanning speed. Powdered samples were reduced *ex situ* in H_2 stream.

Catalytic Tests

The catalysts were evaluated during the selective hydrogenation of 1-heptyne (Fluka, Cat. No. 51950, purity > 98%), 1-pentyne (Aldrich, Cat. No. 627-19-0, purity > 99%) and 1-pentene/1-pentyne mixtures (70:30 and 90:10 vol % ratios; 1-pentene Aldrich, Cat. No. 109-67-1, purity > 98.5%). The operational conditions used were: 150 kPa, 303 K, and a molar ratio of substrate/Pd = 1100 (S/Pd). 50 mL of 2 vol % substrate in toluene (Merck, Cat. No. TX0735-44, purity > 99%) solution using a stainless steel batch reactor coated with polytetrafluoroethylene (PTFE). Agitation of 750 rpm was used in order to eliminate external diffusional limitations. The reagents and

products were analyzed by gas chromatography (GC) with an FID detector and HP INNOWax capillary column of Polyethyleneglycol (PEG).

The Lindlar commercial catalyst (Aldrich, Cat. No. 20,573-7) was used for comparative purposes without any pretreatment as suggested by other authors for the hydrogenation of alkynes[34, 40, 41].

RESULTS AND DISCUSSION

Supports Characterization

The modified alumina support (Al_2O_3-Mg) showed by ICP-OES 5.5 wt % of Mg, being similar to the expected theoretical value, confirming the presence of magnesium surface species in this support. The adsorption-desorption isotherms of Al_2O_3 and Al_2O_3-Mg present a type IV isotherm and a hysteresis loop type H2 associated with mesoporous structure, while $CaCO_3$ support shows a type II isotherm associated with a macroporous or non-porous solid[42] (**Figure S1a**). RX3 support (activated carbon) presents both types I and IV isotherms with a H4 hysteresis loop at higher relative pressures, which is associated with different porosity ranging from micropore to mesopore[43-45] (**Figure S1a**). As reported in a previous work[15]; Al_2O_3, Al_2O_3-Mg and $CaCO_3$ supports showed a S_{BET} of 180, 120 and 4 $m^2\ g^{-1}$ and a pore diameter, d_p, of 9.6, 7.2, and 10.6 nm, respectively. The Al_2O_3-Mg support, presents a reduction in the surface area, which is attributed to the incorporation of Mg species over Al_2O_3 surface, in total accordance with several published reports[46]. Whereas, the S_{BET} values of $CaCO_3$ support is very low, which is consistent with values reported for calcium carbonate[47]. RX3 support shows the highest values of S_{BET} (1,524 $m^2\ g^{-1}$), pore volume (V_p 0.62 $cm^2\ g^{-1}$) and average pore diameter (d_p 26.7 nm) compared to the other supports (**Table S1).** These values are similar to those reported by other authors for this support[44, 48].

The DRIFT-Py spectra of the Al_2O_3, Al_2O_3-Mg and RX3 supports showed the vibrational bands at ca. 1,540 and 1,450 cm^{-1} corresponding to Brönsted and Lewis acidic sites[49], respectively (**Figure S2**). The area under these wavenumber regions were integrated and the ratios Brönsted/ Lewis area were calculated. Al_2O_3 and RX3 supports show higher Brönsted/ Lewis acid site ratios: 0.75 and

0.94, respectively (**Table 2S**), indicating higher concentration of Brönsted acidic sites. While, Al_2O_3-Mg support presents a lower Brönsted/Lewis ratio, 0.13, due to a greater concentration of Lewis acidic sites. These results agree with previously reported [15] data of temperature programmed desorption of pyridine (TPD-Py). Al_2O_3, Al_2O_3-Mg and $CaCO_3$ supports showed by TPD-Py different total acidity 32.6, 63.6 and 1.0 $\mu mol_{Py}\ g^{-1}$, respectively[15]. According to Pyridine DRIFT and TPD γ-Al_2O_3 support had acid sites, mainly strong acidic sites (Brönsted). Al_2O_3-Mg support had the highest Lewis acidic strength due to the incorporation of magnesium species. The $CaCO_3$ support exhibited the lowest or null acidity, which is related to the basic characteristics of this support. In the case of the activated carbon, RX3 support was not analyzed by the TPD-Py technique due to the desorption of CO and CO_2, products of the decomposition of the support between 723 K - 1000 K, which might generate measurement errors in the catalytic methanation detection system. While the DRIFT-Py analysis shows that RX3 presents both Bronsted and Lewis acid sites, mainly Brönsted (**Table S2**).

From the CO and CO_2 desorptions during the TPD-MS analysis of RX3, as the temperature is increased, it is possible to obtain information about the different superficial groups present on the support, which can confer acid characteristics to the support[50-52]. The CO desorption peaks show mainly an evolution from 400-1000 K for the RX3 support, which could be attributed to carbonyl, phenols and quinone groups[50-52] (**Figure S1b**). Besides, in CO_2 evolution with different intensities and peaks are shown obtained for RX3 support assigned to carboxylic anhydride groups and lactone groups on the carbon surface which are more stable systems[53] (**Figure S1b**). The total areas of CO, CO_2 and O_2 calculated from the deconvolution of the signals obtained in the TPD-MS analysis of RX3 (**Table S1**) suggest that the support has a greater amount of functional groups such as: phenols, ethers and carbonyls/quinone as determined by the higher content of released CO compared to the total amount of released CO_2 (carboxylic acid groups, anhydrides and lactones). From these results it can be concluded that the RX3 support has differences in the quantity, nature and stability. These results agree with that observed by DRIFT-Py.

The TPR-H_2 profiles of the supports are used as a reference to compare them with the profiles of the synthesized catalysts. The TPR profile of the supports showed quite similar behavior, showing significant changes from the baseline from 800 K (**Figure S3**). The Al_2O_3 support between 770-900 K an abrupt decrease in the TCD detector signal is observed, after 900 K the signal tends to normalize [38]. This behavior could be attributed to water being evolved, due to a change of phase or sintering of the material as a consequence of the thermal decomposition of this support[54]. For the Al_2O_3-Mg, $CaCO_3$ and RX3 supports the TPR profiles show at high temperatures the reduction of magnesium precursor species $MgSO_4$ (H_2S and SO_3 residual can be generated)[55], decomposition processes of $CaCO_3$ in which CO_2 is produced[56] and hydrogen consumption assigned to the reduction of support surface groups[50], respectively. The area below the peak of hydrogen consumption for RX3 support estimates a number of reducible species of several groups present on the surface of the support, especially oxygenated ones, these results agree with those found by TPD-MS.

Figure S5 shows the XRD diffractograms of the catalysts and their corresponding database references: Pd, MgO, $CaCO_3$, Al_2O_3 and C type graphite. XRD for the Pd/Al–Mg, Pd/Al and Pd/Ca, Lindlar samples present the characteristic of γ-Al_2O_3 and calcium carbonate, respectively **(Figure S5)**. While Pd/RX3 presents characteristic peaks of the C type graphite at $2\theta = 26.4°$. Due to the low concentration of Pd in all the samples (< 1 wt%), well below the detection limit of the XRD technique (> 5 wt %), the characteristic peaks of Pd(111) are overlapped with the peaks of the supports and the presence of Pd crystallites is undetectable. On the Pd/Al–Mg sample, the presence of MgO is detected with low intensity, characteristic peaks at $2\theta = 37°$ and 45°. For the Lindlar catalyst the characteristic peak of Pd (111) is observed at $2\theta = 40.1°$. In spite of the very high Pd load (5 wt %) in the commercial catalyst the pattern is dominated by strong and narrow reflexes of the $CaCO_3$ support. This is consistent with data previously reported by other authors[15, 57].

Catalysts Characterization

Figures 1a and **1b** show respectively the TPD-Py profiles and DRIFT-Py spectra for the catalysts. In the TPD-Py, three regions are marked (**Figure 1a**): Region-I of weak acidity for temperatures between 400 – 600 K, Region-II of medium acidity for temperatures between 600 – 800 K and Region-III of strong acidity for temperatures above 800 K, the integration of these areas give the total amount of acid sites[58-60]. According to different authors [61, 62], the peaks of weak acidity can be attributed to Lewis acid sites, the peaks of moderate acidity to a combination of Lewis and Brönsted acid sites, while strong acid sites would be Brönsted sites. The Pd/Al trace shows a considerable peak in Region-I, and a very pronounced medium acidity peak in the Region-II ca. 723 K; while the strong acidity peak of Region-III is still present. The addition of Mg species to the support significantly modifies the acidic characteristics of the Al_2O_3 support, which can be clearly seen in the TPD-Py profile. The TPD-Py trace of Pd/Al-Mg is shifted to lower temperatures, the area of Region-I is increased, also a medium acidity peak in the Region-II is also observed at 775 K, while the strong acidity peak of Region-III almost disappeared. Besides, Pd/Ca and Lindlar profiles are quite similar, showing a small peak in the Region-II at 690 K for both catalysts. The DRIFT-Py spectra of catalysts (**Figure 1b)** confirm the presence of Brönsted and Lewis acid sites over synthetized catalysts in different concentrations[49]. For Pd/Al Pd/Al-Mg and Pd/RX3 show both peaks corresponding to Brönsted and Lewis acid sites. While, for Pd/Ca a very small peak at 1,450 cm^{-1} (Lewis acid sites) is observed.

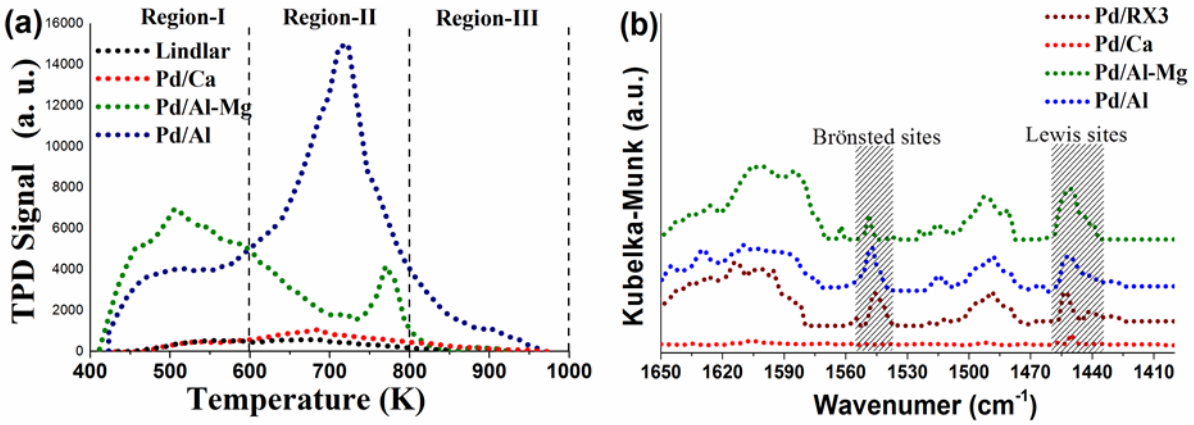

Figure 1. a) TPD-Py analysis and b) DRIFT-Py analysis of the catalysts.

The TPD-Py traces were integrated to obtain total amount of weak Lewis acidity (400- 600 K), mild Lewis/Brönsted acidity (600–800 K) and strong Brönsted acid sites (T > 800 K) and the Brönsted/Lewis acid site ratios obtained by DRIFT-Py were included in **Table 1**. A marked increase in total acidity after palladium addition is observed in TPD-Py analysis of catalysts which could be attributed to the presence of several Pd and chloride residual species, responsible of different types of Lewis and Brönsted acid sites observed also by DRIFT-Py analysis. Pd/Al catalyst shows the highest total acidity compared to other catalysts, also a marked increase of medium acidity is observed. While Pd/Al-Mg catalyst shows that the incorporation of Mg(II) and Pd(II) species over the alumina support, has the greatest effect on the quantity and quality of acidic properties, exhibiting greater weak acidity, but a markedly decrease of medium acidity in comparison to the Pd/Al catalyst. Total, medium and weak acidity of Lindlar and Pd/Ca are the lowest, besides strong acidity is absent in both catalysts. This is mainly due to the basic character of the support. The obtained order of total acidity strength was: Pd/Al >> Pd/Al-Mg >>> Pd/Ca > Lindlar. In **Table 2,** the Brönsted/Lewis acid site ratio of the catalysts obtained by DRIFT-Py, show a similar remaining acid strength to that of fresh support (**Tabla S2**) and this confirms the results observed by TPD-Py.

Table 1. TPD-Py and Brönsted/Lewis Ratio by DRIFT-Py results of the catalysts.

Catalyt	TPD-Py Acid Sites ($\mu mol_{Py}\ g^{-1}$)				DRIFT-Py Brönsted/Lewis Ratio
	Total	Weak	Medium	Strong	
Pd/Al	106.38	37.71	63.54	5.13	0.71
Pd/Al-Mg	82.05	65.89	14.40	1.75	0.11
Pd/Ca	7.02	0.72	6.30	---	--
Pd/RX3	---	---	---	---	1.13
Lindlar	5.26	1.17	4.09	---	--

Figure 2a shows the TPR-H_2 traces of the prepared catalysts. The reduction of species at temperatures below 250 K cannot be observed due to equipment limitations. Pd/Al and Pd/Al–Mg catalysts exhibit an initial reduction peak at 308 and 348 K, respectively. This peak at low temperatures is assigned to the reduction of bulk PdO species to metallic palladium[63]. For these peaks, a shift to higher temperatures is observed in this order: Pd/Al < Pd/Al–Mg which could indicate higher interaction forces between the metallic species with the support, consistent with the amount of weak acidity (related to Lewis sites). **Figure 2a** also shows that during TPR analysis, Pd/Ca and Pd/RX3 have a negative peak at 326 and 344 K, respectively, due to the release of hydrogen from the decomposition of the β-phase of Pd hydrides (β-PdH) formed during the reduction of PdO at low temperatures[63]. These species interact weakly with the support and thus Pd can be easily reduced.

Besides, several peaks at 382, 437, 452 and 580 K for synthetized catalysts are also observed in **Figure 2a**. These peaks are assigned to the hydrogen consumption, due to the reduction of $Pd_xO_yCl_z$ oxychlorinated species or the reduction of Pd^{2+} ions stabilized by adjacent Cl^- remaining after the calcination process[15]. For Pd/Al-Mg and Pd/Ca a gradual increase peak is observed at temperatures higher than 700 K. These peaks are attributed to the reduction of the remaining sulfate magnesium precursor (SO_4^{2-}) that generates residual H_2S or SO_3[55] and to the decomposition of $CaCO_3$[56, 64],

respectively. For Pd/RX3 catalyst the TPR-H_2 results show a broad peak with a maximum between 700 - 981 K, this consumption is assigned to the reduction of surface groups on the catalyst[50]; this peak was also observed in the TPR-H_2 profile of the support (**Figure S3**). The reduction profiles of the catalysts suggest that palladium is at least partly in the Pd^0 metal state after the reduction treatment before the catalytic tests.

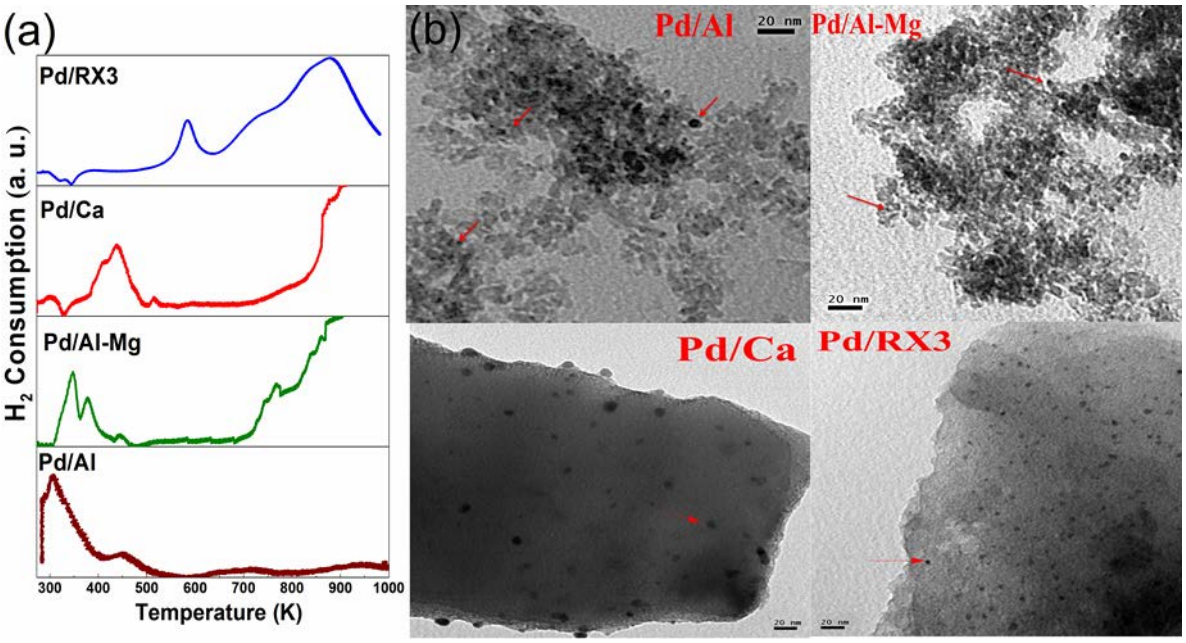

Figure 2. a) TPR- H_2 profile of the synthetized catalysts and b) TEM images.

Table 2. Pd and Cl loadings, average particle size (d_{TEM}) by TEM, dispersion (D) and XPS results.

Sample	ICP		d_{TEM}	D	XPS				
	Pd	Cl			Pd $3d_{5/2}$ BE (eV)			Pd/X*	Cl/Pd
	(wt %)		(nm)	(%)	Pd^0	$Pd^{\delta+}$	Pd^{n+}	($\%^{at}/_{at}$)	($\%^{at}/_{at}$)
Pd/Al	0.86	0.41	3.8	30	335.2$^{(60\%)}$		337.5$^{(40\%)}$	0.0040	4.15
Pd/Al-Mg	0.73	0.22	6.2	19	334.9$^{(72\%)}$	336.1$^{(28\%)}$		0.0065	2.32
Pd/Ca	0.90	0.55	10.0	11	334.8$^{(45\%)}$	336.1$^{(33\%)}$	337.5$^{(23\%)}$	0.0539	3.95
Pd/RX3	0.74	0.11	7.1	16	335.3$^{(74\%)}$		337.0$^{(26\%)}$	0.0348	0.78
Lindlar	5.00	--	46.0	2.5	335.2$^{(69\%)}$		336.9$^{(31\%)}$	0.2430	--

* Pd/X: superficial atomic ratio, where X=Al for Pd on Al_2O_3 and Al_2O_3-Mg; X=Ca for Pd on $CaCO_3$ and Lindlar; and X=C for Pd on RX3.

Table 2 shows the Pd and Cl content measured by chemical analysis (ICP), average particle size (d_{TEM}), dispersion (D) determined by TEM and XPS results for the Pd/Al, Pd/Al–Mg, Pd/Ca, Pd/RX3 and Lindlar catalysts. The commercial catalyst has a high Pd content of 5 wt %. For the synthetized catalysts a Pd mass content between 0.73 and 0.9 wt %, similar to the theoretical values, was determined by ICP analysis. A metal loading of 2.7 wt % of Mg was detected on Pd/Al–Mg. Besides, **Table 2** shows the residual bulk chlorine content of the catalysts after calcination and reduction pretreatments. The bulk Cl^- detected by ICP in all the catalysts, are consistent with the surface chloride species ($Pd_xCl_yO_z$) observed by TPR-H_2 analysis in **Figure 2a**. Higher Cl content in Pd/Ca and Pd/Al is found; while for Pd/Al-Mg and Pd/RX3, the lowest values are observed. The high charge density of Ca^{2+} would favor the adsorption of chloride species over the $CaCO_3$ support. For the catalysts based on alumina and modified alumina, the presence of superficial Mg species might have an influence on the amount of final chlorine, the half bulk chloride is observed for the

Pd/Al-Mg catalyst compared to Pd/Al, indicating that the presence of magnesium may help a lower presence of residual chlorine species.

Figure 2b and **S4** show TEM images and particle size distribution of the catalysts, respectively. **Table 2** reports the average particle size (d_{TEM}) as determined by TEM according to **Equation I**.

$$d_{TEM} = \frac{\sum n_i . d_i^3}{\sum n_i . d_i^2} \qquad \textbf{(Eq. I)}$$

Particle size values confirm the presence of nanoparticles between 3.8 and 10 nm for all synthesized catalysts. Particle size order increases as follows: Pd/Al < Pd/Al-Mg < Pd/RX3 < Pd/Ca, respectively. Pd/Al, Pd/Al-Mg and Pd/RX3 catalysts have a Gaussian distribution which indicates uniform nanoparticle distribution. While for the Pd/Ca catalyst, a Gaussian trend is not observed, which indicates a less uniform distribution (**Figure S4**).

The metallic dispersions D were calculated considering the spherical particle model adopted by Paryjczak and Szymura[65], these values are included in **Table 2**. The highest dispersion is observed for the Pd/Al catalyst (≈ 30%), while for Pd/Al-Mg, Pd/Ca and Pd/RX3 lower dispersions are obtained, between 19-11%. These results may be indicative of greater interaction between the precursor $PdCl_2$ salt at pH = 1 with the Al_2O_3 and Al_2O_3-Mg supports during wet impregnation due to their higher acidic characteristics (**Table 1**). Similarly, the lower specific surface area and pore volume of the $CaCO_3$ support may be the responsible for the low dispersion of the metallic sites over this support. In the case of RX3 activated carbon, the presence of different surface functional groups could be responsible for the interaction with the precursor complex, reducing its metallic dispersion. The Lindlar commercial catalyst has the highest average particle size (46 nm) and the lowest dispersion (2.5%), as shown in **Table 2**. This can be attributed to the high loading of Pd deposited on a support of low surface area and acidity, thus promoting a greater agglomeration of the particles in the pore mouths.

Figure 3 shows the XPS spectra of the Pd *3d* region of synthetized catalysts (pretreated in hydrogen at 573 K) and Lindlar catalysts. This figure presents the Pd $3d_{5/2}$ and $3d_{3/2}$ signals separated by approximately 5 eV, in accordance with literature values[66]. The points are the experimental data and the curves beneath are the corresponding deconvoluted peaks informed on **Table 2**. The Pd/Al and Pd/RX3 present two Pd $3d_{5/2}$ peaks at 335.2-335.3 eV and 337.0-337.5 eV, which can be assigned to Pd^0 and Pd^{n+} (with *n* close to 2) electrodeficient oxychlorinated species formed during the calcination pretreatment[30, 38]. The deconvolution of the Pd $3d_{5/2}$ signal for the Pd/Al-Mg catalysts shows the presence of two peaks at 334.9 eV and 336.1; assigned to Pd^0 and $Pd^{\delta+}$ (with $0< \delta < 2$)[23, 39]. While, Pd/Ca catalyst presents three peaks for Pd $3d_{5/2}$ at 334.8, 336.1 and 337.5 eV, assigned to Pd^0, $Pd^{\delta+}$ and Pd^{n+} , respectively[30, 38, 39]. Besides the Lindlar catalyst presents two peaks at 335.2 and 336.9 eV attributed to Pd^0 and Pd^{n+}. **Figure 3** also shows the XPS spectrum of the Mg *1s* region of the Pd/Al-Mg sample with a peak located at 1304.95 eV, which is attributed to MgO surface species [39] also detected by the ICP analysis. Deconvolution of the XPS spectra of the synthetized catalysts, also shows a peak at ca. 198.5 eV that corresponds to Cl $2p_{3/2}$ associated with surface chloride species [39] not completely eliminated after reduction.

Values of the superficial Pd/X and Cl/Pd atomic ratios are also shown in **Table 2.** The Pd/Al superficial atomic ratio is higher for Pd/Al–Mg in comparison to Pd/Al (0.0065 and 0.0040, respectively); this could be explained to the preferential deposition of Pd on the pore mouth as the pore diameter diminished. For the Pd/Ca and Lindlar catalyst the Pd/Ca superficial atomic ratio is the highest (0.0539 and 0.2430). This could be related to the differences in BET area and the very low pore volume (V_p) that favor a high content of palladium at a surface level. For Pd/RX3 catalysts the Pd/C superficial atomic ratio is intermediate (0.0348) due to higher interactions of Pd species with the support. On the other hand, Cl/Pd surface atomic ratios decrease in the following order: Pd/Al ≥ Pd/Ca > Pd/Al–Mg > Pd/RX3. The residual chlorine content in the catalysts after reduction could be explained by the different superficial $Pd_xO_yCl_z$ species detected on each catalyst by XPS,

ICP and TPR-H_2. The presence of Cl^- could also have some influence on the metallic dispersion, as well as on the performance of the catalysts.

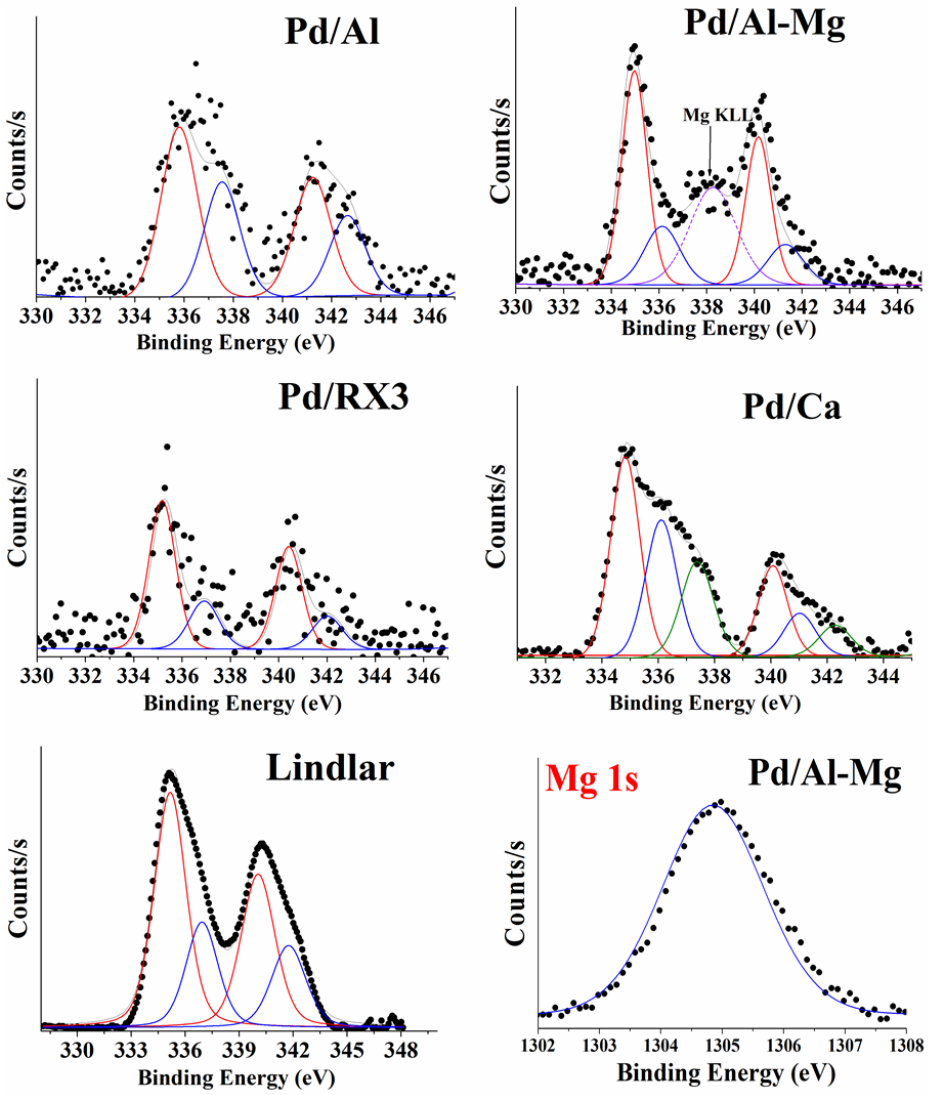

Figure 3. XPS spectra of the Pd *3d* region of all catalysts and the Mg *1s* region of Pd/Al-Mg.

CATALYTIC TESTS

Hydrogenation of Pure 1-Heptyne and 1-Pentyne

The selectivities (S) to 1-alkene/n-alkane as a function of total conversions (X) during the hydrogenation of pure 1-heptyne or 1-pentyne, are shown in **Figures 4a** and **b**, respectively. As shown in both Figures, all the catalysts are active for the hydrogenation of 1-heptyne or 1-pentyne.

Besides, initially all catalysts are high selectively to 1-heptene (**Figure 4a**, ca. 98%), but after X ≈ 30% these values are higher than the Lindlar commercial catalyst. At higher conversions the selectivity to 1-heptene of Pd/Al and Pd/RX3 decreases up to 65 % when X= 99.9%. In addition, for Pd/RX3 a gradual increase in the selectivity to heptane is observed from X = 20 %, while in Pd/Al the increase in the selectivity to heptane is observed at high conversion values. Besides, Pd/Al-Mg and Pd/Ca catalysts presente selectivities to 1-heptene ca. ≈ 90% quite higher than Lindlar catalyst, 82%, while the selectivities to heptane are rather stable after X= 30%.

On the other hand, during 1-pentyne hydrogenation (**Figure 4b**), Pd/Al and Pd/Al-Mg catalysts have selectivities to 1-pentene ≥ 90%, higher to that of Lindlar commercial catalyst. For Pd/Ca or Pd/RX3 catalysts, initially high selectivity values are obtained (≥ 90 %), but when X ≥ 70 %, the selectivities begin to decrease, reaching values ca.70 and 78%, respectively for X= 99.9 %.

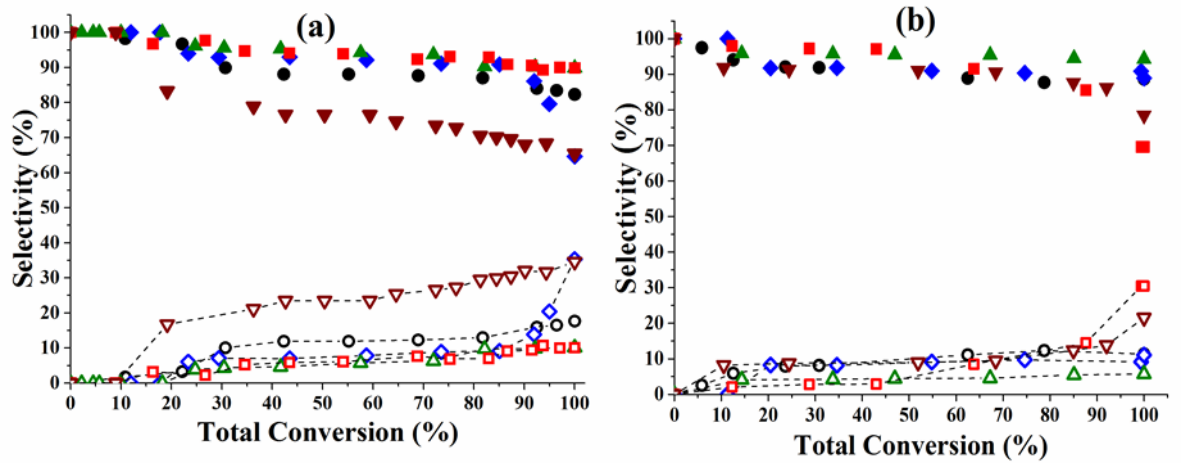

Figure 4. Selectivity to 1-alkene or n-alkane vs Total conversion (%) during hydrogenation of (a) 1-Heptyne (b) 1-Pentyne, for Pd/Al (♦,◊), Pd/Al-Mg (▲,△), Pd/Ca (■,□), Pd/RX3 (▼,▽) and Lindlar (●,○). Filled symbols 1-alkene, opened symbols n-alkane.

In **Figure 5** are shown the values of selectivities at isoconversion conditions (X= 99.9 %), values of the initial reaction rate (mass based r^0) and TOF for all the evaluated catalysts during the

hydrogenation of pure 1-heptyne and 1-pentyne. The initial reaction rate of the pure alkynes was calculated using the following formula (**Equation II**):

$$r^0 = \frac{V.C^0}{W_{Pd}}.\left(\frac{\partial X}{\partial t}\right)_{t=0} \qquad \textbf{(Eq. II)}$$

r^0 is the initial reaction rate of the alkyne [mol g_{Pd}^{-1} min^{-1}]. $(\partial X/\partial t)_{t=0}$ is the tangent value of the plot of alkyne total conversion versus time at t = 0. C^0 is the initial concentration of alkyne [mol L^{-1}], W_{Pd} the mass of palladium [g_{Pd}], V the reaction volume [L] and t the reaction time [min]. The turnover frequency (TOF) values were obtained for the catalysts as reported for several authors[23, 67, 68], using initial reaction rates determined in **Equation III** and dispersion values were calculated considering the spherical particle model, both values are indicated in **Table 2**:

$$TOF = \frac{V.C^0.MW_{Pd}}{W_{Pd}.D}\left(\frac{\partial X}{\partial t}\right)_{t=0} = r^0\frac{MW_{Pd}}{D} \qquad \textbf{(Eq. III)}$$

Where TOF is expressed in min^{-1}, MW_{Pd} is the molecular weight of palladium and D the dispersion.

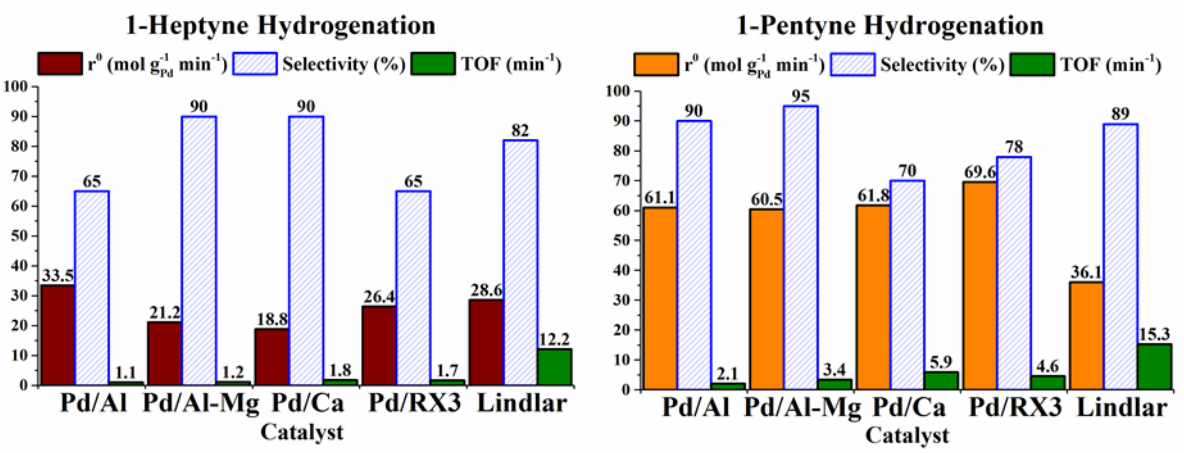

Figure 5. Initial reaction rates, selectivities to the corresponding alkene and TOF, during 1-Heptyne and 1-Pentyne hydrogenations at isoconversion of 99.9 %.

For the hydrogenation of the 1-heptyne, the following initial reaction rate order was found: Pd/Al > Lindlar > Pd/RX3 > Pd/Al–Mg > Pd/Ca. While for the hydrogenation of the 1-pentyne, the following initial reaction rate order is found: Pd/RX3 > Pd/Ca ≥ Pd/Al ≥ Pd/Al–Mg > Lindlar. The TOF values for 1-heptyne and 1-pentyne hydrogenation were quite similar between: Pd/Al and Pd/Al-Mg or between Pd/Ca and Pd/RX3, in contrast with TOF values of Lindlar catalyst.

Figure 5 shows in all cases, regardless of the catalyst, the hydrogenation reaction rates of 1-pentyne are greater than those of 1-heptyne. Because of the smaller size of 1-pentyne, its adsorption on electrodeficient palladium oxychloride sites is more sterically and geometrically favored than 1-heptyne, giving a higher hydrogenation rate. So, the 1-pentyne molecule, with a shorter carbonaceous chain, could interact with more active sites than 1-heptyne. As shown in **Figure 5** the synthesized catalysts presented much higher or similar values of initial reaction rate of 1-pentyne than the Lindlar catalyst. During the hydrogenation of 1-heptyne, the synthesized catalysts presented a comparable initial reaction rate, quite similar to that of Lindlar catalyst. In terms of selectivities to 1-heptene or 1-pentene Pd/Al–Mg catalysts showed the highest values: 90 and 95%, respectively, greater to that obtained using the Lindlar commercial catalyst. While Pd/Al and Pd/RX3 had the lowest selectivity to 1-heptene, and Pd/Ca and Pd/RX3 had the lowest selectivity to 1-pentene.

High conversions and selectivities are achieved with lower Pd loading than the commercial Lindlar catalyst, ca. 1 vs. 5 wt %, respectively. The Pd synthesized catalysts showed higher or similar values of r^0 than the Lindlar catalyst during the hydrogenation of 1-heptyne and 1-pentyne (pure compounds). The good activity of the synthesized catalysts could be related to: a) geometrical effect due to the small active sizes 3.8 – 10 nm (**Table 2**), b) electronic effect originated by the high content of Pd^0 or $Pd^{\delta+}$ metallic sites, d^{10} rich in electrons as found by XPS (**Table 2**), that promotes the dissociative adsorption of hydrogen [69-71] and c) electronic effect between the acidic Lewis sites of the catalysts as determined by TPD and DRIFT of pyridine (**Table 1**). So, differences in activity

could be mainly attributed to the influence of the geometric and electronic effects generated by different supports and chlorinated precursor.

The selectivities of all the catalysts were excellent, these could be attributed to acidic Lewis sites that promote the adsorption and desorption of the alkyne and alkene (Lewis bases). It was observed that Pd/Al-Mg had the greatest selectivity to 1-heptene and 1-pentene, and the high content of weak acidic groups (Lewis acid sites). It has been reported[26, 32, 72], that Mg species increase selectivity, stability and improves catalytic properties due to the decrease in deactivation and poisoning on the surface of the catalyst. Pd/Ca had high selectivity to 1-heptene and moderate selectivity to 1-pentene, this could be attributed to the presence of Pd^{n+} and Ca^{2+} (hard Lewis acid sites) that promotes the adsorption of the alkyne triple bond (basic Lewis sites) and desorption of the alkene. On the other hand, the Pd catalysts supported on Al_2O_3 and RX3, initially showed very high selectivity to 1-heptene but, at a total conversion of 99.9 % decreased up to 65 %. Regarding the acidic properties, both catalysts had high acidity, mainly strong and medium acidity due to the presence of Brönsted acid sites in the case of Pd/Al and acidic functional groups, Brönsted type, in the case of Pd/RX3.

1-Pentene Purification in 1-Pentene/1-Pentyne Streams

In this work the 1-pentene purification of the stream C_5 (1-pentene/1-pentyne mixture) was chosen as a model reaction to evaluate the catalytic performance and selectivity of the synthesized catalysts. In order to observe the effect of the alkene concentration in the 1-pentene/1-pentyne mixture, two different relationships were evaluated: 70:30 and 90:10 vol %.

1-Pentene Purification in 1-Pentene/1-Pentyne Stream 70:30 vol %

Figure 6 shows the molar concentration of the substrates and products as a function of time during the hydrogenation of 1-pentene/1-pentyne mixture, 70:30 vol %. In general, a decrease in the total concentration of 1-pentyne is observed for all the catalysts evaluated. Further, the progressive

increase of the molar concentration of 1-pentene until total conversion of the alkyne was also observed in the Figure, indicating that the catalysts were selective for the hydrogenation of 1-pentyne. The most active catalyst was Pd/Al, followed by Pd/Ca and Pd/RX3. While Pd/Al-Mg and Lindlar catalysts were the less active. In **Figure 6** can be observed that Pd/Al-Mg and Pd/Ca favored the highest formation of 1-pentene with less production of pentane. Pd/Al and Pd/RX3 favored overhydrogenation of 1-pentyne and the hydrogenation of 1-pentene. Additionally, the presence of isomerization product 2-pentene was only observed for Pd/Al catalyst.

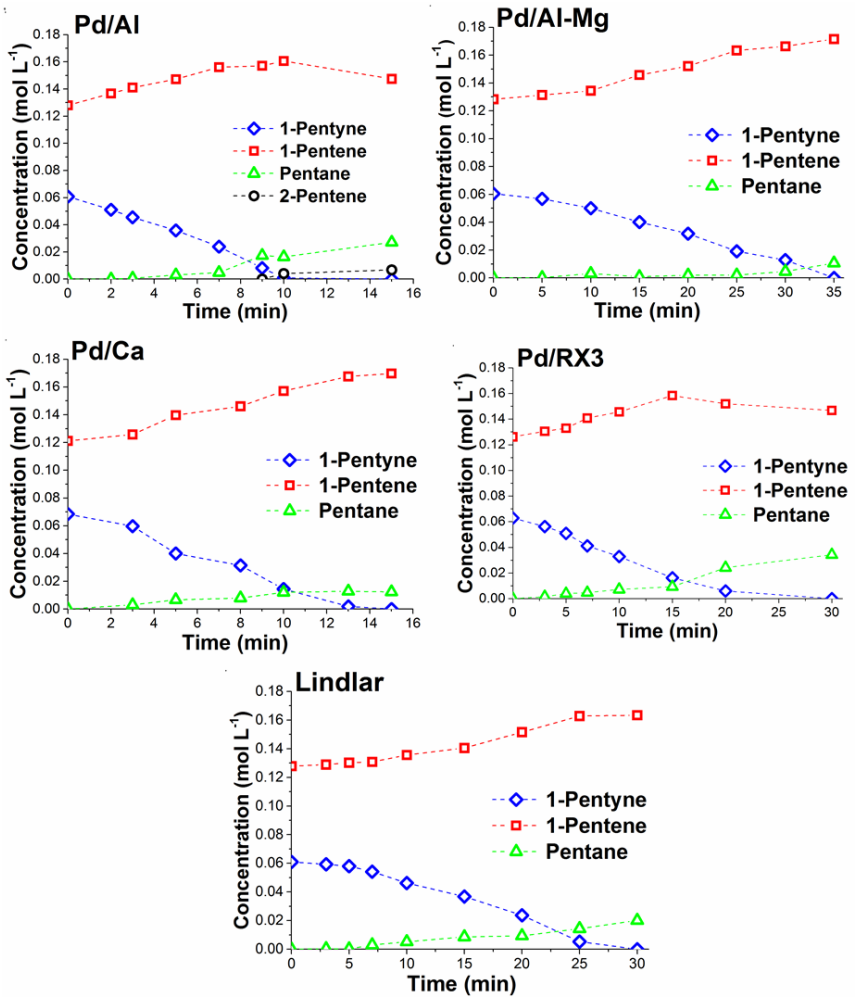

Figure 6. Concentration of reactants and products (mol L^{-1}) as a function of time (min) during the purification of 1-pentene/1-pentyne mixture (70:30 vol %).

Figure 7 contains values of selectivities at isoconversion conditions (X= 99.9 %), values of the initial reaction rate (mass based r^0) and TOF for all the evaluated catalysts during the 1-Pentene Purification. For the purification of 1-pentene/1-pentyne stream (70:30 vol %), the following initial reaction rate order was found: Pd/Al >> Pd/Ca >> Pd/RX3 >> Pd/Al–Mg > Lindlar. Additionally, the Pd/Al-Mg and Pd/Ca catalysts had the highest selectivity to 1-pentene during the hydrogenation of the mixture with values of 94 and 93%, respectively. While for Pd/Al and Pd/RX3 a progressive decrease in selectivity was observed throughout the reaction, obtaining moderate selectivities compared to the other catalysts, close to 80%.

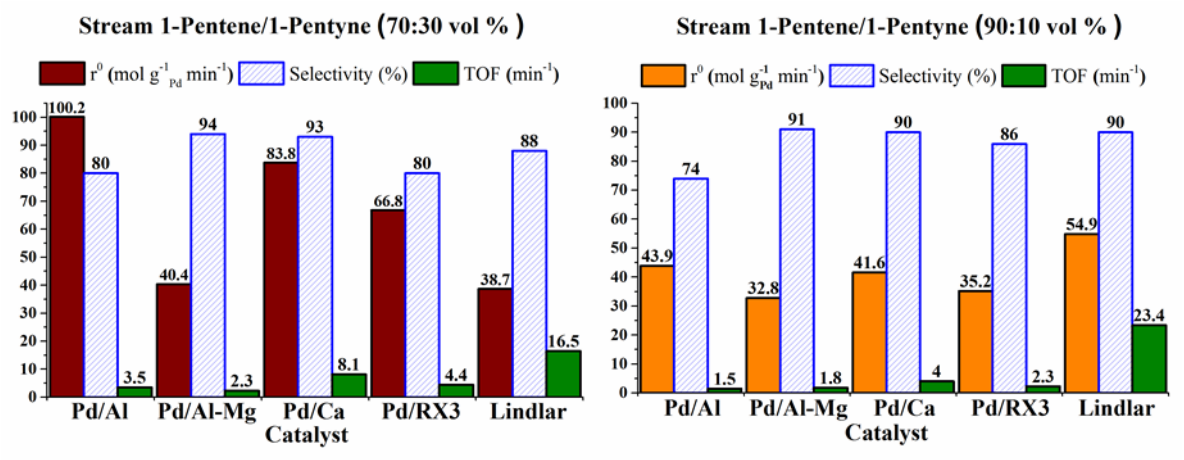

Figure 7. Initial reaction rates, selectivities to 1-pentene and TOF, during the olefin purification in 1-Pentene/1-Pentyne mixtures, 70:30 and 90:10 vol % at X = 99.9 %.

1-Pentene Purification in 1-Pentene/1-Pentyne Stream 90:10 vol %

Figure 8 shows the molar concentration profiles of reagents and products as a function of time during the hydrogenation of the stream 1-Pentene/1-Pentyne 90:10 vol %. In this Figure was observed mainly the consumption of 1-pentyne, the progressive increase in the concentration of 1-pentene was less marked due to the high initial concentration of 1-pentene in the mixture. Otherwise, the presence of pentane in different concentrations was observed for all the catalysts. In **Figure 8** similar performance was observed for Pd/Al, Pd/Ca and Pd/RX3 reaching total conversion ca 30-40 minutes. Besides, Pd/Al–Mg reached the total conversion at the longest reaction time, 80

min. It was observed that Pd/RX3 and Pd/Al favored the overhydrogenation of the alkyne and the hydrogenation of 1-pentene. Pd/Al was the only catalyst that also favored the production of 2-pentene. Pd/Al-Mg, Pd/Ca and Lindlar showed a slight decrease in the concentration of 1-pentene as the reaction advanced, forming the lowest amount of pentane in the mixture.

Very similar r^0 values were observed for the synthesized catalysts during the purification of 90:10 vol % stream (**Figure 7**). The following order of initial reaction rates was found: Lindlar > Pd/Al > Pd/Ca > Pd/RX3 ≥ Pd/Al–Mg. Otherwise, it can be noted that during the purification of C_5 streams, the prepared catalysts showed lower r^0 and TOF values at higher concentration of alkene (90:10) than those obtained during the purification of 70:30 stream. The different values of TOF could be attributed to lower Pd loading and particle sizes than the commercial Lindlar catalyst (**Figure 7**). Besides, it was evidenced the high selectivity to 1-pentene of Pd/Ca and Pd/Al-Mg (90 and 91%, respectively) very similar to that of Lindlar catalyst; while the selectivities of Pd/Al and Pd/RX3 were moderate (74 and 86%, respectively). From these results it can be affirmed that it is possible to purify 1-pentene from a C_5 olefin stream of 1-Pentene/1-Pentyne mixture 90:10 vol % with the synthesized catalysts, as the selectivities are similar or higher to that of Lindlar commercial catalyst.

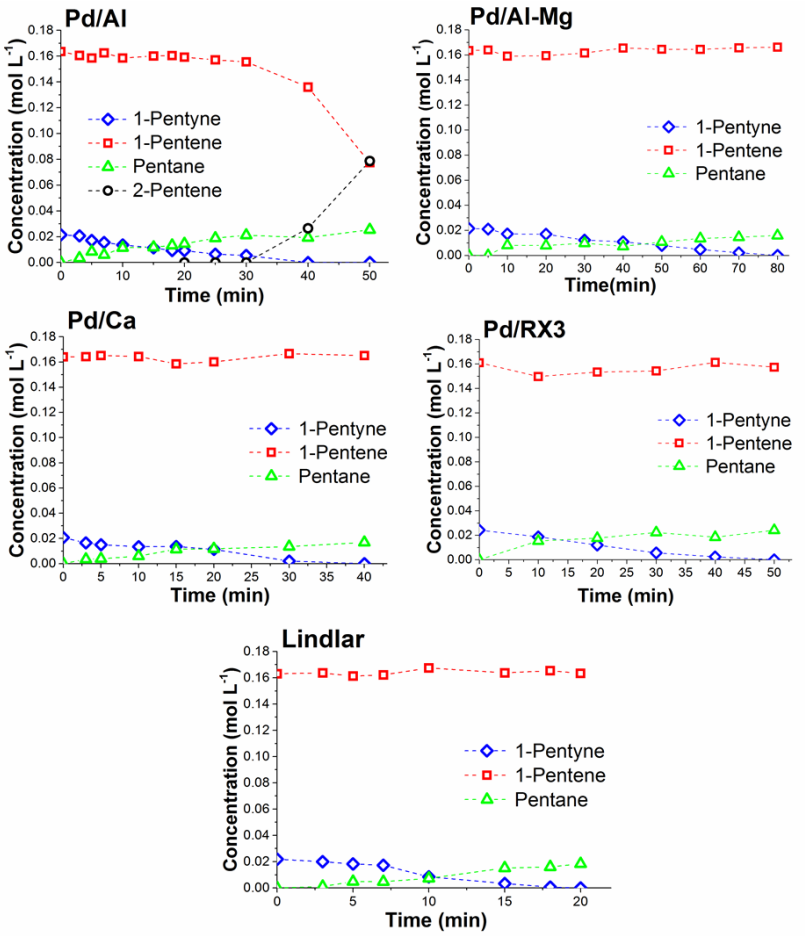

Figure 8. Concentration of reactants and products (mol L^{-1}) as a function of time (min) during the purification of 1-pentene/1-pentyne mixture (90:10 vol %).

The results indicate that all the synthesized Pd catalysts were active during 1-pentene purification of C_5 olefin at 70:30 and 90:10 vol % streams. High selectivities were observed for the evaluated catalysts, suggesting that their physicochemical properties prevent to some extent the processes of overhydrogenation and isomerization. This could be directly related to different surface interactions, electronic and geometric effects of the synthesized catalysts using different supports and chlorinated precursor. As previously discussed in hydrogenation of pure alkynes, small particle sizes (geometric effects) and Pd^0 active sites (electronic effects) are responsible for the high activity. Pd/Al showed the highest activity; which correlates with the TEM results that showed the smallest particle size (≤

3.8 nm) and greatest dispersion. While Pd/Ca, Pd/RX3 and Pd/Al-Mg show a relationship regarding small particle sizes (between 6.2 to 10 nm) and moderate dispersions (**Table 2**). In addition, the presence of superficial Pd^0 and $Pd^{\delta+}$ or Pd^{n+} species electronically modified with Cl^- (oxychloride specie as determined by ICP, XPS and TPR analysis). These results showed better or similar values of initial hydrogenation rate than that of the commercial Lindlar catalyst, which has very large particle sizes (46 nm) and superficially Pd^0 and Pd^{n+} species electronically modified with Pb, a very toxic element. Selectivity values to the desired product (1-alkene) between 74-94% were obtained for the two purified 1-pentene/1-pentyne streams. Surface acidity of the catalysts (Lewis and Bronsted sites), MgO or $Pd_xCl_yO_z$ surface species contribute to promote the desorption/adsorption of 1-pentene during the olefin purification being the responsible of the selectivity[73]. The obtained results indicate that the Pd catalysts supported on Al_2O_3-Mg and $CaCO_3$ show the best results in terms of selectivity for the purification of 1-pentene of the two mixtures, 70:30 or 90:10 vol %. Both catalysts showed high selectivity values, $S \geq 91\%$. Pd/RX3 showed a high selectivity to the alkene, $\geq 80\%$. While Pd/Al catalyst with Al_2O_3 support presented lower selectivity values compared to the other catalysts (≥ 74 %), which indicates that its properties favored the processes of overhydrogenation and isomerization. The 2-pentene isomerization product was only observed in the Pd/Al catalyst, favored by the strong acidic sites (Brönsted) of this catalyst. Additionally, the results of concentration of substrates and products as a function of time demonstrated the preferential hydrogenation of C≡C in the evaluated mixtures reaching its total conversion, indicating the excellent selectivities of the catalysts. When comparing the results obtained during the purification of 1-pentene with those obtained in the hydrogenation reaction of pure alkynes, a quite different behavior was observed, due to the differences of active sites and acidity properties of the catalysts. The literature indicates that it is important to have better catalytic properties to mainly improve the selectivity to the alkene, because in this type of alkene/alkyne purification reaction, at high concentration of alkyne, the alkyne efficiently blocks the re-absorption of alkene over some active sites[9, 74]. However, some catalytic properties such as: type of support, surface acidity, particle

size, dispersion, type of active sites among others, can influence undesired processes such as overhydrogenation or isomerization reactions of alkenes[6, 9, 75, 76].

Scheme 1 summarizes the proposed interaction between palladium precursor with the different supports used in the synthesis of the catalysts. Initially, the chloride palladium precursor $[PdCl_4]^{2-}$ at pH = 1 was impregnated over different supports that offer different physicochemical characteristics. After the pretreatment conditions, Pd^0, $Pd^{\delta+}$ and Pd^{n+} nanoparticles were found superficially on the fresh catalysts. Residual chloride and $Pd_xCl_yO_z$ species were determined in all the catalysts, especially on Pd/Al and Pd/Ca. $Pd^{\delta+}Cl_yO_z$, $Pd^{n+}Cl_yO_z$, Mg^{2+} and/or Ca^{2+} species, and carbonaceous acidic groups have different electro-deficiency (Lewis acid sites) which could be increased by metal-support interaction.

Besides, **Scheme 2** shows proposed hydrogenations mechanisms during the purification reaction of 1-pentene in the C_5 streams over supported Pd catalysts. A brief explanation for each catalyst mechanism is now presented:

(2,a) Catalysts with Al_2O_3-Mg and $CaCO_3$ supports: During the purification reaction of 1-pentene, the 1-pentyne or 1-pentene of the mixture are preferentially **π** or **σ** adsorbed on the $Pd^{\delta+}$, Pd^{n+}, Mg^{2+} or Ca^{2+} electron-deficient sites. While H_2 molecules are adsorbed and dissociated on Pd^0 sites due to the interaction of its d^{10} filled orbital with the empty antibonding σ orbital of H_2 [83]. On the other hand, the **π** or **σ** interaction of the adsorbed 1-alkyne is promoted by the presence of Lewis acidic sites and also facilitates the desorption of the desired 1-alkene in the mixture, preventing its further overhydrogenation or isomerization, improving selectivity and olefin purification.

(2,b) Catalysts with Al_2O_3 and RX3 supports: During the purification reaction of 1-pentene, the 1-pentyne or 1-pentene of the mixture are **π** or **σ** strongly adsorbed on the Pd^{n+} active sites or on surface groups of the activated carbon. The dihydrogen molecules are dissociatively adsorbed on Pd^0 sites due to their high availability of electrons; besides, the Brönsted acidic sites promotes an

extra hydrogen atom that increase the hydrogenation reaction rate but also promotes overhydrogenation, isomerization or polymerization reactions, decreasing the quality of the purification of 1-alkene and the selectivity of the process.

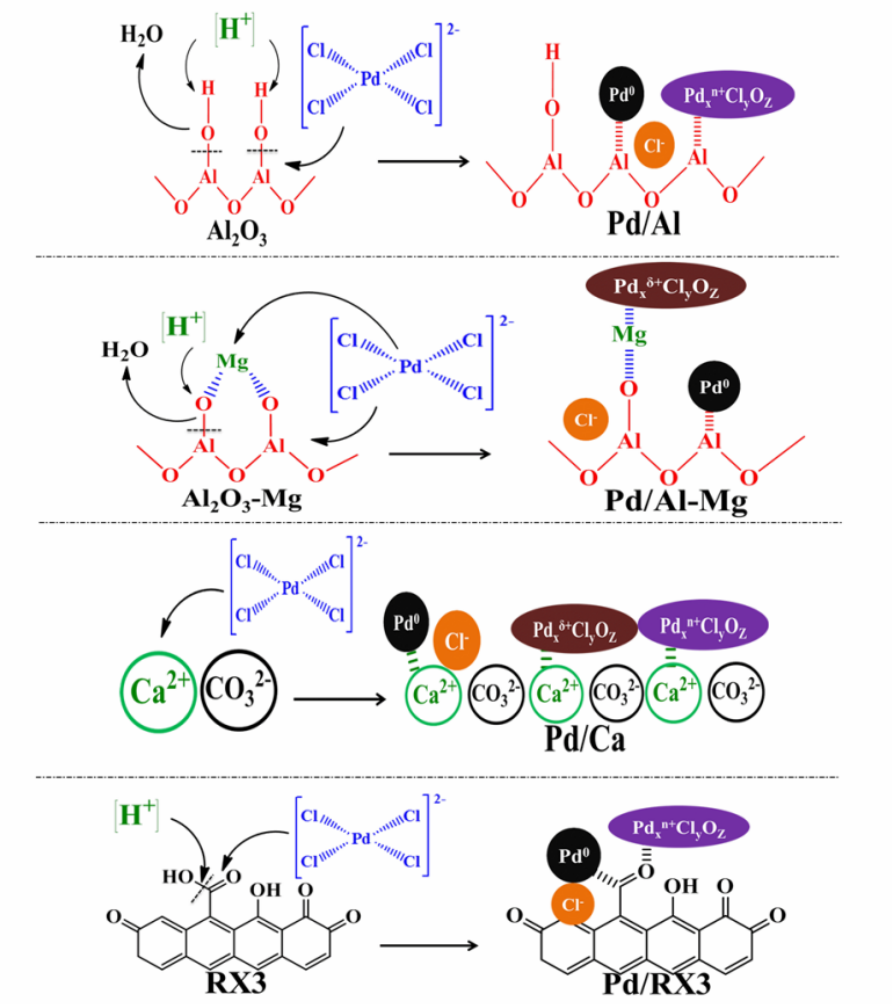

Scheme 1. Proposed mechanisms of interactions between palladium precursor and the different supports used for the synthesis of catalysts (not scaled).

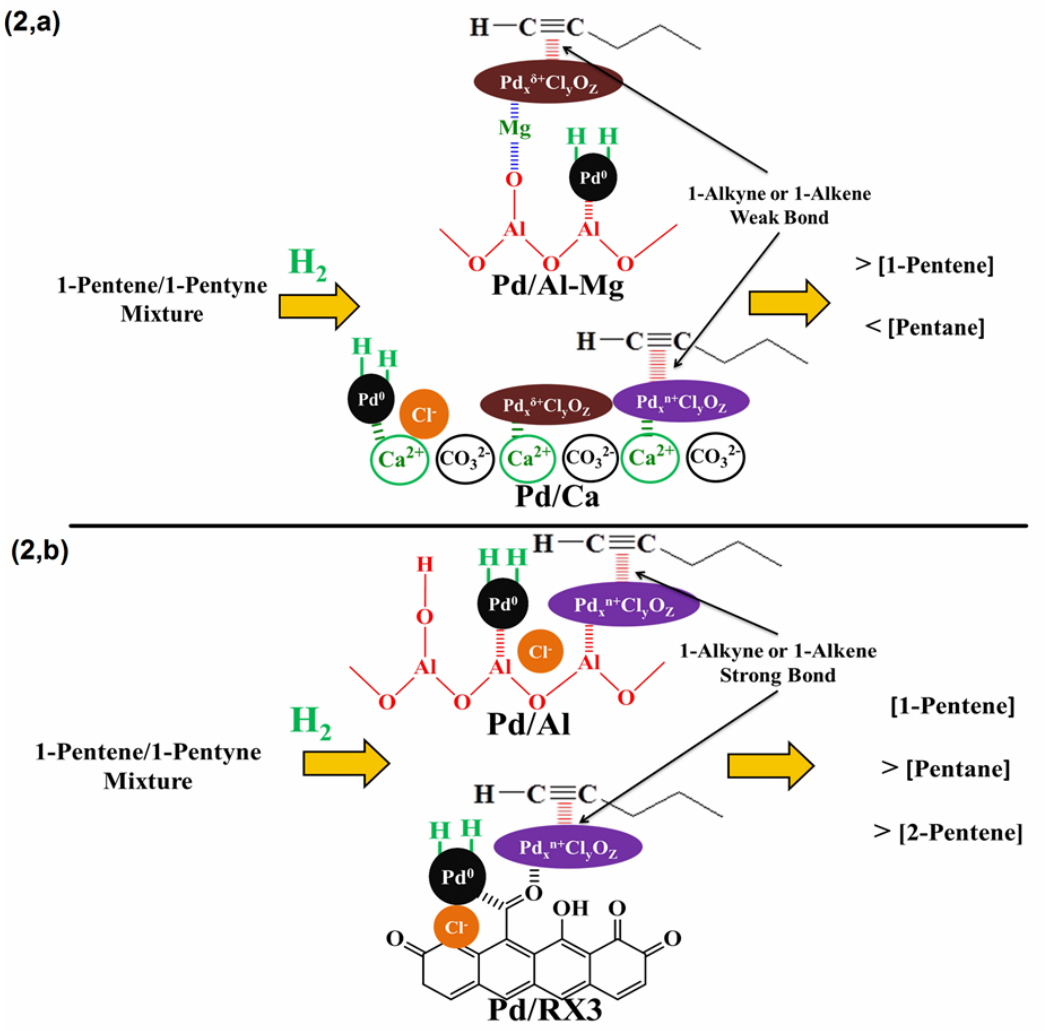

Scheme 2. Proposed hydrogenation mechanism during the purification reaction of 1-pentene in the C_5 streams over supported Pd catalysts (not scaled).

CONCLUSIONS

Pd nanoparticles were deposited on four different supports: γ-Al_2O_3, γ-Al_2O_3 modified with Mg, $CaCO_3$ and activated carbon RX3 using palladium chloride ($PdCl_2$) as a precursor salt. The catalysts were evaluated in the 1-pentene purification of alkene/alkyne streams (70:30 and 90:10 % vol) and during the selective hydrogenation of medium chain terminal alkynes (C_7 and C_5, pure compounds). Lindlar commercial catalyst was used as a reference. The role of the support, the geometric and

electronic properties during the hydrogenation reactions have the major influence on the selectivity and over the catalytic performance.

XPS and TPR-H_2 analysis revealed that all the synthetized catalysts had a high concentration of superficial Pd^0 nanoparticles and different amounts of $Pd^{\delta+}O_yCl_z$ or $Pd^{n+}O_yCl_z$ oxychlorinated species. These nanoparticles of Pd were generated due to the interaction of the precursor employed ($PdCl_2$) and the support (Metal-Support Interaction, MSI) during the synthesis of the catalysts.

The TPD-Py results showed that Pd catalysts supported on Al_2O_3-Mg and $CaCO_3$ present mostly weak acidity, Lewis type. While for the catalyst of Pd supported in Al_2O_3 presents mostly moderate or strong acidity, Brönsted type. For Pd/RX3, the TPD-MS results showed the presence of different surface groups on the activated carbon surface.

The catalytic results showed that the prepared catalysts were highly active and selective to the 1-alkene production. In this context, it was possible to purify 1-pentene from the alkyne / alkene evaluated streams, and it was also feasible to selectively hydrogenate the pure alkynes, 1-heptyne and 1-pentyne. Selectivity values were indeed higher than those of the Lindlar commercial catalyst. Smaller particle sizes, Pd^0 and weak acidity favor high activity and selectivity to the alkene.

The Brönsted acidic sites of Pd/Al and Pd/RX3 promote an extra hydrogen atom that increases the hydrogenation reaction rate but also promotes overhydrogenation, isomerization or polymerization reactions, decreasing the selectivity of the process. On the other hand, Lewis acid sites of Pd/Al-Mg and Pd/Ca catalysts, promote the π or σ interaction of the adsorbed 1-alkyne and also facilitates the desorption of the desired 1-alkene in the mixture, preventing its further overhydrogenation or isomerization, improving selectivity and olefin purification.

Low loaded Pd catalysts supported on Al_2O_3-Mg and $CaCO_3$ (Pd/Al-Mg, Pd/Ca) can be used for the purification of medium or large terminal alkenes at mild reaction conditions as an alternative to the Lindlar commercial catalyst.

ACKNOWLEDGMENT

The financial support provided by UNL (Grants CAI+D), CONICET (Grant PIP 11220130100457CO) and ANPCyT (Grants PICT 2016 and 2020) are acknowledged. L. García thanks Minciencias (Call 860, for Doctorates abroad 2019).

REFERENCES

1. Dobson NA, Eglinton G, Krishnamurti M, Raphael RA and Willis RG, Selective catalytic hydrogenation of acetylenes. *Tetrahedron* **16**: 16-24 (1961). http://dx.doi.org/10.1016/0040-4020(61)80050-1
2. Thomas SP and Greenhalgh MD, 8.16 Heterogeneous Hydrogenation of CC and CC Bonds A2 - Knochel, Paul, in Comprehensive Organic Synthesis II (Second Edition). Elsevier, Amsterdam, pp. 564-604 (2014). http://dx.doi.org/10.1016/B978-0-08-097742-3.00818-1
3. Ibhadon AO KS, The Reduction of Alkynes Over Pd-Based Catalyst Materials- A Pathway to Chemical Synthesis. *Journal of Chemical Engineering & Process Technology* **9**: 376 (2018). DOI:10.4172/2157-7048.1000376
4. Bazzazzadegan H, Kazemeini M and Rashidi AM, A high performance multi-walled carbon nanotube-supported palladium catalyst in selective hydrogenation of acetylene-ethylene mixtures. *Applied Catalysis A: General* **399**: 184-190 (2011). https://doi.org/10.1016/j.apcata.2011.03.055
5. Tew MW, Janousch M, Huthwelker T and van Bokhoven JA, The roles of carbide and hydride in oxide-supported palladium nanoparticles for alkyne hydrogenation. *Journal of Catalysis* **283**: 45-54 (2011). https://doi.org/10.1016/j.jcat.2011.06.025
6. Lederhos CR, Badano JM, Carrara N, Coloma-Pascual F, Almansa MC, Liprandi D and Quiroga M, Metal and Precursor Effect during 1-Heptyne Selective Hydrogenation Using an Activated Carbon as Support. *The Scientific World Journal* **2013**: 9 (2013). http://dx.doi.org/10.1155/2013/528453
7. Werner Bonrath JM, Jan Schütz, and Bettina Wüstenberg TN, Hydrogenation in the Vitamins and Fine Chemicals Industry – An Overview. *InTech*, **Hydrogenation.**: 66-90 (2012). DOI: 10.5772/48751
8. Mastalir Á, Quiroga M, Szabó T, Zsigmond Á and Dékány I, Catalytic investigation of PdCl2(TDA)2 immobilized on hydrophobic graphite oxide in the hydrogenation of 1-pentyne and the Heck coupling reaction. *Reaction Kinetics, Mechanisms and Catalysis* **113**: 61-68 (2014). https://doi.org/10.1016/j.cattod.2010.10.012
9. Garcia PE, Lynch AS, Monaghan A and Jackson SD, Using modifiers to specify stereochemistry and enhance selectivity and activity in palladium-catalysed, liquid phase hydrogenation of alkynes. *Catalysis Today* **164**: 548-551 (2011). https://doi.org/10.1016/j.cattod.2006.04.002
10. Boronoev MP, Zolotukhina AV, Ignatyeva VI, Terenina MV, Maximov AL and Karakhanov EA, Palladium Catalysts Based on Mesoporous Organic Materials in Semihydrogenation of Alkynes. *Macromolecular Symposia* **363**: 57-63 (2016). DOI: 10.1002/masy.201500184
11. Nijhuis TA, van Koten G and Moulijn JA, Optimized palladium catalyst systems for the selective liquid-phase hydrogenation of functionalyzed alkynes. *Applied Catalysis A: General* **238**: 259-271 (2003). https://doi.org/10.1016/S0926-860X(02)00372-1
12. Nikoshvili LZ, Makarova AS, Lyubimova NA, Bykov AV, Sidorov AI, Tyamina IY, Matveeva VG and Sulman EM, Kinetic study of selective hydrogenation of 2-methyl-3-butyn-2-ol over Pd-containing hypercrosslinked polystyrene. *Catalysis Today* **256**: 231-240 (2015). https://doi.org/10.1016/j.cattod.2015.02.033

13. Hu J, Zhou Z, Zhang R, Li L and Cheng Z, Selective hydrogenation of phenylacetylene over a nano-Pd/α-Al2O3 catalyst. *Journal of Molecular Catalysis A: Chemical* **381**: 61-69 (2014). https://doi.org/10.1016/j.molcata.2013.10.008
14. Livingstone SE, Comprehensive Inorganic Chemistry, in The Chemistry of Ruthenium, Rhodium, Palladium, Osmium, Iridium and Platinum. Pergamon, pp. ii (1973). https://doi.org/10.1016/S0926-860X(00)00889-9
15. Cordoba Misael, Pascual Fernando, Quiroga Mónica and Cecilia L, Olefin Purification and Selective Hydrogenation of Alkynes with Low Loaded Pd Nanoparticle Catalysts. *Industrial & Engineering Chemistry Research* **58**: 17182-17194 (2019). DOI: 10.1021/acs.iecr.9b02081
16. Setiawan I and Cavell KJ, Removal of unstaturated contaminants from an industrial C4-stream using Cu/SiO2 catalysts: Subsequent testing of the purified stream with an alkyne sensitive catalyst system. *Applied Catalysis A: General* **131**: 225-241 (1995). https://doi.org/10.1016/0926-860X(95)00145-X
17. Zhao D, Liu X, Wang D, Zhou X, Liu Z and Yuan W, Hydrogenation of acetylenic contaminants over Ni-Based catalyst: Enhanced performance by addition of silver. *Journal of Cleaner Production* **220**: 289-297 (2019). https://doi.org/10.1016/j.jclepro.2019.01.339
18. McCue AJ, Guerrero-Ruiz A, Ramirez-Barria C, Rodríguez-Ramos I and Anderson JA, Selective hydrogenation of mixed alkyne/alkene streams at elevated pressure over a palladium sulfide catalyst. *Journal of Catalysis* **355**: 40-52 (2017). https://doi.org/10.1016/j.jcat.2017.09.004
19. Pei GX, Liu XY, Wang A, Lee AF, Isaacs MA, Li L, Pan X, Yang X, Wang X, Tai Z, Wilson K and Zhang T, Ag Alloyed Pd Single-Atom Catalysts for Efficient Selective Hydrogenation of Acetylene to Ethylene in Excess Ethylene. *ACS Catalysis* **5**: 3717-3725 (2015). https://doi.org/10.1021/acscatal.5b00700
20. Borodziński A and Bond GC, Selective Hydrogenation of Ethyne in Ethene-Rich Streams on Palladium Catalysts. Part 1. Effect of Changes to the Catalyst During Reaction. *Catalysis Reviews* **48**: 91-144 (2006). https://doi.org/10.1080/01614940500364909
21. McCue AJ, Gibson A and Anderson JA, Palladium assisted copper/alumina catalysts for the selective hydrogenation of propyne, propadiene and propene mixed feeds. *Chemical Engineering Journal* **285**: 384-391 (2016). https://doi.org/10.1016/j.cej.2015.09.118
22. Lederhos CR, Badano JM, Quiroga ME, L'Argentière PC and Coloma-Pascual F, Influence of ni addition to a low-loaded palladium catalyst on the selective hydrogenation of 1-heptyne. *Química Nova* **33**: 816-820 (2010). https://doi.org/10.1590/S0100-40422010000400010
23. Maccarrone MJ, Lederhos CR, Torres G, Betti C, Coloma-Pascual F, Quiroga ME and Yori JC, Partial hydrogenation of 3-hexyne over low-loaded palladium mono and bimetallic catalysts. *Applied Catalysis A: General* **441–442**: 90-98 (2012). http://dx.doi.org/10.1016/j.apcata.2012.07.016
24. Lindlar H and Dubuis R, Palladium Catalyst for Partial Reduction of Acetylenes, in Organic Syntheses. John Wiley & Sons, Inc. (2003). http://dx.doi.org/10.1002/0471264180.os046.27
25. Lindlar H, Ein neuer Katalysator für selektive Hydrierungen. *Helvetica Chimica Acta* **35**: 446-450 (1952). DOI: 10.1002/hlca.19520350205
26. He Y, Fan J, Feng J, Luo C, Yang P and Li D, Pd nanoparticles on hydrotalcite as an efficient catalyst for partial hydrogenation of acetylene: Effect of support acidic and basic properties. *Journal of Catalysis* **331**: 118-127 (2015). https://doi.org/10.1016/j.jcat.2015.08.012
27. Cao Y, Sui Z, Zhu Y, Zhou X and Chen D, Selective Hydrogenation of Acetylene over Pd-In/Al2O3 Catalyst: Promotional Effect of Indium and Composition-Dependent Performance. *ACS Catalysis* **7**: 7835-7846 (2017). http://dx.doi.org/10.1021/acscatal.7b01745
28. Anderson JA, Mellor J and Wells RPK, Pd catalysed hexyne hydrogenation modified by Bi and by Pb. *Journal of Catalysis* **261**: 208-216 (2009). https://doi.org/10.1016/j.jcat.2008.11.023
29. Crespo-Quesada M, Cárdenas-Lizana F, Dessimoz A-L and Kiwi-Minsker L, Modern Trends in Catalyst and Process Design for Alkyne Hydrogenations. *ACS Catalysis* **2**: 1773-1786 (2012). https://doi.org/10.1021/cs300284r
30. Cárdenas-Lizana F, Hao Y, Crespo-Quesada M, Yuranov I, Wang X, Keane MA and Kiwi-Minsker L, Selective Gas Phase Hydrogenation of p-Chloronitrobenzene over Pd Catalysts: Role of the Support. *ACS Catalysis* **3**: 1386-1396 (2013). https://doi.org/10.1021/cs4001943
31. Pan C-J, Tsai M-C, Su W-N, Rick J, Akalework NG, Agegnehu AK, Cheng S-Y and Hwang B-J, Tuning/exploiting Strong Metal-Support Interaction (SMSI) in Heterogeneous Catalysis. *Journal of*

the Taiwan Institute of Chemical Engineers **74**: 154-186 (2017). https://doi.org/10.1016/j.jtice.2017.02.012

32. Stakheev AY and Kustov LM, Effects of the support on the morphology and electronic properties of supported metal clusters: modern concepts and progress in 1990s. *Applied Catalysis A: General* **188**: 3-35 (1999). https://doi.org/10.1016/S0926-860X(99)00232-X
33. Chen Z, Chen J and Li Y, Metal–organic-framework-based catalysts for hydrogenation reactions. *Chinese Journal of Catalysis* **38**: 1108-1126 (2017). https://doi.org/10.1016/S1872-2067(17)62852-3
34. Albers PW, Möbus K, Frost CD and Parker SF, Characterization of β-Palladium Hydride Formation in the Lindlar Catalyst and in Carbon-Supported Palladium. *The Journal of Physical Chemistry C* **115**: 24485-24493 (2011). http://dx.doi.org/10.1021/jp205951c
35. Carrara N, Betti C, Coloma-Pascual F, Almansa MC, Gutierrez L, Miranda C, Quiroga ME and Lederhos CR, High-Active Metallic-Activated Carbon Catalysts for Selective Hydrogenation. *International Journal of Chemical Engineering* **2018**: 11 (2018). https://doi.org/10.1155/2018/4307308
36. Betti C, Badano J, Maccarrone MJ, Mazzieri V, Vera C and Quiroga M, Effect of the sequence of impregnation on the activity and sulfur resistance of Pt–Ni/γ-Al2O3 bimetallic catalysts for the selective hydrogenation of styrene. *Applied Catalysis A: General* **435-436**: 181-186 (2012). https://doi.org/10.1016/j.apcata.2012.06.001
37. Betti C, Carrara N, Badano J, Lederhos C, Vera C and Quiroga M, MORE ACTIVE AND SULFUR RESISTANT BIMETALLIC Pd-Ni CATALYSTS. *Química Nova* **41**: 151-156 (2018). https://doi.org/10.21577/0100-4042.20170152
38. Badano JM, Quiroga M, Betti C, Vera C, Canavese S and Coloma-Pascual F, Resistance to Sulfur and Oxygenated Compounds of Supported Pd, Pt, Rh, Ru Catalysts. *Catalysis Letters* **137**: 35-44 (2010). https://doi.org/10.1007/s10562-010-0336-x
39. NIST X-Ray Photoelectron Spectroscopy D, NIST X-ray photoelectron spectroscopy database NIST standard reference database 20, Version 3.5 (Web version), National Institute of Standards and Technology, USA, 2007.
40. Lederhos CR, Maccarrone MJ, Badano JM, Torres G, Coloma-Pascual F, Yori JC and Quiroga ME, Hept-1-yne partial hydrogenation reaction over supported Pd and W catalysts. *Applied Catalysis A: General* **396**: 170-176 (2011). https://doi.org/10.1016/j.apcata.2011.02.011
41. Vilé G, Almora-Barrios N, Mitchell S, López N and Pérez-Ramírez J, From the Lindlar Catalyst to Supported Ligand-Modified Palladium Nanoparticles: Selectivity Patterns and Accessibility Constraints in the Continuous-Flow Three-Phase Hydrogenation of Acetylenic Compounds. *Chemistry – A European Journal* **20**: 5926-5937 (2014). DOI: 10.1002/chem.201304795
42. Pawelec B, Venezia AM, La Parola V, Cano-Serrano E, Campos-Martin JM and Fierro JLG, AuPd alloy formation in Au-Pd/Al2O3 catalysts and its role on aromatics hydrogenation. *Applied Surface Science* **242**: 380-391 (2005). https://doi.org/10.1016/j.apsusc.2004.09.004
43. Leofanti G, Padovan M, Tozzola G and Venturelli B, Surface area and pore texture of catalysts. *Catalysis Today* **41**: 207-219 (1998). https://doi.org/10.1016/S0920-5861(98)00050-9
44. Díaz-Auñón JA, Román-Martínez MC, Salinas-Martínez de Lecea C, L'Argentière PC, Cagnola EA, Liprandi DA and Quiroga ME, [PdCl2(NH2(CH2)12CH3)2] supported on an active carbon: effect of the carbon properties on the catalytic activity of cyclohexene hydrogenation. *Journal of Molecular Catalysis A: Chemical* **153**: 243-256 (2000). https://doi.org/10.1016/S1381-1169(99)00355-6
45. Thommes M, Kaneko K, Neimark AV, Olivier JP, Rodriguez-Reinoso F, Rouquerol J and Sing KSW, Physisorption of gases, with special reference to the evaluation of surface area and pore size distribution (IUPAC Technical Report). *Pure and Applied Chemistry* **87**: 1051-1069 (2015). DOI:10.1515/pac-2014-1117
46. Skalny J and Hearn N, 13 - Surface Area Measurements, in Handbook of Analytical Techniques in Concrete Science and Technology, ed by Ramachandran VS and Beaudoin JJ. William Andrew Publishing, Norwich, NY, pp. 505-527 (2001). https://doi.org/10.1016/B978-081551437-4.50016-3
47. Ahsan T, The surface properties of pure and modified precipitated calcium carbonate by adsorption of nitrogen and water vapor. *Colloids and Surfaces* **64**: 167-176 (1992). https://doi.org/10.1016/0166-6622(92)80096-K
48. Durán-Valle CJ, Madrigal-Martínez M, Martínez-Gallego M, Fonseca IM, Matos I and Botelho do Rego AM, Activated carbon as a catalyst for the synthesis of N-alkylimidazoles and imidazolium ionic liquids. *Catalysis Today* **187**: 108-114 (2012). https://doi.org/10.1016/j.cattod.2011.12.021

49. McCue AJ, Mutch GA, McNab AI, Campbell S and Anderson JA, Quantitative determination of surface species and adsorption sites using Infrared spectroscopy. *Catalysis Today* **259**: 19-26 (2016). https://doi.org/10.1016/j.cattod.2015.03.039
50. Cordoba M, Miranda, Cristian, , Lederhos C, Coloma-Pascual Fernando, Ardila Alba, Fuentes GA, Pouilloux Y and Ramírez A, Catalytic Performance of Co3O4 on Different Activated Carbon Supports in the Benzyl Alcohol Oxidation. *Catalysts* **7**: 384 (2017). DOI: 10.3390/catal7120384
51. Aksoylu AE, Madalena M, Freitas A, Pereira MFR and Figueiredo JL, The effects of different activated carbon supports and support modifications on the properties of Pt/AC catalysts. *Carbon* **39**: 175-185 (2001). DOI: 10.1016/S0008-6223(00)00102-0
52. Román-Martínez MC, Cazorla-Amorós D, Linares-Solano A and de Lecea CS-M, Tpd and TPR characterization of carbonaceous supports and Pt/C catalysts. *Carbon* **31**: 895-902 (1993). https://doi.org/10.1016/0008-6223(93)90190-L
53. Rodrigues EG, Pereira MFR, Chen X, Delgado JJ and Órfão JJM, Influence of activated carbon surface chemistry on the activity of Au/AC catalysts in glycerol oxidation. *Journal of Catalysis* **281**: 119-127 (2011). https://doi.org/10.1016/j.jcat.2011.04.008
54. Lee HH, Deactivation of catalysts *AIChE Journal* **31**: 523-523 (1985). DOI: 10.1002/aic.690310334
55. Scheidema MN and Taskinen P, Decomposition Thermodynamics of Magnesium Sulfate. *Industrial & Engineering Chemistry Research* **50**: 9550-9556 (2011). DOI: 10.1021/ie102554f
56. Padeste C, Reller A and Oswald HR, The influence of transition metals on the thermal decomposition of calcium carbonate in hydrogen. *Materials Research Bulletin* **25**: 1299-1305 (1990). https://doi.org/10.1016/0025-5408(90)90088-J
57. Tripathi B, Paniwnyk L, Cherkasov N, Ibhadon AO, Lana-Villarreal T and Gómez R, Ultrasound-assisted selective hydrogenation of C-5 acetylene alcohols with Lindlar catalysts. *Ultrasonics Sonochemistry* **26**: 445-451 (2015). https://doi.org/10.1016/j.ultsonch.2015.03.006
58. Sadeghpour P and Haghighi M, High-temperature and short-time hydrothermal fabrication of nanostructured ZSM-5 catalyst with suitable pore geometry and strong intrinsic acidity used in methanol to light olefins conversion. *Advanced Powder Technology* **29**: 1175-1188 (2018). https://doi.org/10.1016/j.apt.2018.02.009
59. Auroux A, Monaci R, Rombi E, Solinas V, Sorrentino A and Santacesaria E, Acid sites investigation of simple and mixed oxides by TPD and microcalorimetric techniques. *Thermochimica Acta* **379**: 227-231 (2001). https://doi.org/10.1016/S0040-6031(01)00620-7
60. Fals J, García JR, Falco M and Sedran U, Performance of Equilibrium FCC Catalysts in the Conversion of the SARA Fractions in VGO. *Energy & Fuels* **34**: 16512-16521 (2020).DOI: 10.1021/acs.energyfuels.0c02804
61. Topsøe N-Y, Pedersen K and Derouane EG, Infrared and temperature-programmed desorption study of the acidic properties of ZSM-5-type zeolites. *Journal of Catalysis* **70**: 41-52 (1981). https://doi.org/10.1016/0021-9517(81)90315-8
62. Zakaria ZY, Linnekoski J and Amin NAS, Catalyst screening for conversion of glycerol to light olefins. *Chemical Engineering Journal* **207-208**: 803-813 (2012). https://doi.org/10.1016/j.cej.2012.07.072
63. Ferrer V, Moronta A, Sánchez J, Solano R, Bernal S and Finol D, Effect of the reduction temperature on the catalytic activity of Pd-supported catalysts. *Catalysis Today* **107–108**: 487-492 (2005). http://doi.org/10.1016/j.cattod.2005.07.059
64. L'Vov BV, Mechanism of thermal decomposition of alkaline-earth carbonates. *Thermochimica Acta* **303**: 161-170 (1997). https://doi.org/10.1016/S0040-6031(97)00261-X
65. Paryjczak T and Szymura JA, Electron microscopic and chemisorption comparison studies on the metal dispersion of Pd, Rh, and Ir supported catalysts. *Zeitschrift für anorganische und allgemeine Chemie* **449**: 105-114 (1979). DOI: 10.1002/zaac.19794490111
66. Wagner CD and Muilenberg GE, Handbook of X-ray Photoelectron Spectroscopy: A Reference Book of Standard Data for Use in X-ray Photoelectron Spectroscopy. Perkin-Elmer (1979).
67. Bartholomew CH and Farrauto RJ, Fundamentals of Industrial Catalytic Processes. Wiley (2011).
68. Zhang P, Sui Y, Xiao G, Wang Y, Wang C, Liu B, Zou G and Zou B, Facile fabrication of faceted copper nanocrystals with high catalytic activity for p-nitrophenol reduction. *Journal of Materials Chemistry A* **1**: 1632-1638 (2013). http://dx.doi.org/10.1016/j.apcata.2012.07.016

69. Teschner D, Révay Z, Borsodi J, Hävecker M, Knop-Gericke A, Schlögl R, Milroy D, Jackson SD, Torres D and Sautet P, Understanding Palladium Hydrogenation Catalysts: When the Nature of the Reactive Molecule Controls the Nature of the Catalyst Active Phase. *Angewandte Chemie International Edition* **47**: 9274-9278 (2008). DOI: 10.1002/anie.200802134
70. Maccarrone Juliana, Torres Gerardo, Lederhos Cecilia, Betti Carolina, Badano Juan, Quiroga Mónica and Juan Y, Kinetic Study of the Partial Hydrogenation of 1-Heptyne over Ni and Pd Supported on Alumina, Hydrogenation, in Hydrogenation, ed by Iyad Karamé I (2012). DOI: 10.5772/48699
71. Kauffman GB, Inorganic Chemistry (Shriver, Duward F.; Atkins, P. W.; Cooper, H. Langford). *Journal of Chemical Education* **67**: A221 (1990). DOI: 10.1021/ed067pA221.1
72. Liu Y, Zhao J, He Y, Feng J, Wu T and Li D, Highly efficient PdAg catalyst using a reducible Mg-Ti mixed oxide for selective hydrogenation of acetylene: Role of acidic and basic sites. *Journal of Catalysis* **348**: 135-145 (2017). https://doi.org/10.1016/j.jcat.2017.02.020
73. Howeizi J, Taghvaei-Ganjali S, Malekzadeh M, Motiee F and Sahebdelfar S, Effect of preparation parameters on properties and performance of Pd/Al2O3 catalyst in saturation of olefins. *Research on Chemical Intermediates* **45**: 3165-3181 (2019). DOI: 10.1007/s11164-019-03785-5
74. Segura Y, López N and Pérez-Ramírez J, Origin of the superior hydrogenation selectivity of gold nanoparticles in alkyne + alkene mixtures: Triple- versus double-bond activation. *Journal of Catalysis* **247**: 383-386 (2007). https://doi.org/10.1016/j.jcat.2007.02.019
75. Karakhanov E, Maximov A, Terenina M, Vinokurov V, Kulikov L, Makeeva D and Glotov A, Selective hydrogenation of terminal alkynes over palladium nanoparticles within the pores of amino-modified porous aromatic frameworks. *Catalysis Today* (2019). https://doi.org/10.1016/j.cattod.2019.05.028
76. Hou R, Porosoff MD, Chen JG and Wang T, Effect of oxide supports on Pd–Ni bimetallic catalysts for 1,3-butadiene hydrogenation. *Applied Catalysis A: General* **490**: 17-23 (2015). https://doi.org/10.1016/j.apcata.2014.11.001